High Resolution Optical Coherent-Channel Analyzer Using Balanced-Coherent Detection and Temperature-Tuned DFB Laser as Local Oscillator

by

Rejoy Isaac

BEng, University of Victoria, 2008

A Thesis Submitted in Partial Fulfillment
of the Requirements for the Degree of

MASTER OF APPLIED SCIENCE

in the Department of Electrical and Computer Engineering

Supervisory Committee

High Resolution Optical Coherent-Channel Analyzer Using Balanced-Coherent Detection and Temperature-Tuned DFB Laser as Local Oscillator

by

Rejoy Isaac
BEng, University of Victoria, 2008

Supervisory Committee

Dr. Thomas E. Darcie, **Supervisor**
(Department of Electrical and Computer Engineering)

Dr. Sudhakar Ganti, **Departmental Member**
(Department of Computer Science)

Dr. Peter Driessen, **Departmental Member**
(Department of Electrical and Computer Engineering)

Dr. Peter Wild, **Outside Member**
(Department of Mechanical Engineering)

Abstract

Supervisory Committee

Dr. Thomas E. Darcie, **Supervisor**
(Department of Electrical and Computer Engineering)

Dr. Sudhakar Ganti, **Departmental Member**
(Department of Computer Science)

Dr. Peter Driessen, **Departmental Member**
(Department of Electrical and Computer Engineering)

Dr. Peter Wild, **Outside Member**
(Department of Mechanical Engineering)

The rapid increase in demand for bandwidth in optical networks over the last two decades has led to the development of wavelength division multiplexing where multiple channels are transmitted simultaneously at different wavelengths over a single optical-fiber to maximize the usage of the bandwidth available in fiber. Increasing demand for bandwidth has led to narrower channel spacing and the use of advanced modulation schemes that are more spectrally efficient than traditional on-off keying techniques [1]. Nonlinearities and dispersion effects in fiber accumulate over a long distance and can adversely affect the quality of a channel. Hence the ability to measure detailed features of the optical spectrum is crucial to study the performance of a communication link. A conventional optical spectrum analyzer (OSA) based on a diffraction grating has a wide wavelength or frequency scanning range, but suffers from poor frequency resolution. The narrowest resolution bandwidth reported for a grating based OSA is ~0.06nm or 7.5GHz

at 1550nm [1]. Various spectral features of interest, such as the transmission spectrum of a laser and modulation spectrum of a channel require sub-picometer resolution, which cannot be achieved by conventional methods using a diffraction grating.

High resolution spectrum analyzers (HRSAs) have been built based on heterodyne detection where a portion of the optical spectrum is converted to radio-frequency (RF) with DC corresponding to the local-oscillator (LO) central frequency [3-6]. This is a common technique used in RF-spectrum analyzers. The resolution bandwidth is determined by the electrical bandwidth of the optical receiver. The lowest resolution bandwidth reported is of the order of tens of MHz [6]. Widespread implementation of these instruments however, has been limited owing to their cost and size, one of the major factors being the external cavity (ECT) lasers used as the local-oscillator source in such instruments.

We have built a coherent-channel analyzer (CCA) based on balanced coherent detection using a commercial distributed-feedback (DFB) laser as the LO. The use of a DFB laser for the CCA has the potential of reducing the cost of the instrument by at least one-tenth of the price of an HRSA. In this thesis we describe the working of the CCA. We provide an end-to-end system model, analyze the resolution and sensitivity performance of the system, and demonstrate a frequency resolution of 100MHz over the DFB tuning range of 200GHz with a sensitivity of -95dBm. The CCA provides a practical, cost and size effective alternative to the HRSA at the cost of tunability.

Table of Contents

List of Tables

List of Figures

Glossary of terms

OSA	Optical Spectrum Analyzer
HRSA	High-Resolution Spectrum Analyzer based on coherent detection
BOSA	High-Resolution Optical Spectrum Analyzer based on Stimulated Brillouin Scattering built by Aragon Photnics.
CCA	Coherent Channel Analyzer based on Balanced Coherent Detection using a DFB laser as the local oscillator
RBW	Resolution Bandwidth: describes the frequency resolution limit of a spectrum analyzer
VBW	Video Bandwidth: bandwidth of the output signal of the RF power detector.
RF	Radio Frequency
IF	Intermediate Frequency
DFB	Distributed Feedback (Laser)
ECT	External Cavity (Laser)
SHD	Self-Homodyne Detection
BW	Bandwidth
LO	Local Oscillator: reference signal which is combined with the input signal in a coherent receiver.

Acknowledgments

I would like to express my sincere gratitude to everyone who contributed to the completion of this project.

Thanks to my supervisor Dr. Thomas E. Darcie for his constant support and guidance along the way. A special thanks to Dr. Jinye Zhang for sharing his expertise and helping with various experiments. I would like to thank all the students and members of the Optical Systems and Technology Laboratory (OSTL) for their friendship and support.

Funding for this work was provided by NSERC, Canadian Foundation for Innovation and BC Knowledge Development Fund, to whom I express my gratitude.

Finally, I would like to thank my parents who have always stood by my side, offering words of encouragement and for their prayers that have been my strength.

1.0 Introduction

1.1 Fiber Optic Communication Channel Analysis

The last two decades have seen a tremendous growth in the area of fiber optic communication systems leading to a rapid increase in the data rates from 45Mbps to 1Tb/s over up to 10,000km fiber link [7]. Two major technologies instrumental in sparking this revolution in fiber optic communication systems are optical amplifiers and Wavelength Division Multiplexing (WDM).

Optical Amplifiers enabled the amplification of optical signal to be done optically. One such optical amplifier is the erbium doped fiber amplifier (EDFA) which amplifies the optical signal using a fiber doped with rare-earth metals such as Erbium ions and an optical pump signal. This addressed the loss issue in fibers and increased the distance between repeaters that regenerate the signal after converting it from the optical to the electric domain for loss and dispersion compensation. WDM technology enabled the transmission of multiple carriers (channels) with different wavelengths over a single fiber link. This led to a greater utilization of the large bandwidth available in the optical fiber.

Various undesirable effects due to dispersion and non-linearities in fiber accumulate with the transmission of an optical pulse over a long distance. Dispersion in optical fiber caused by different propagation velocities for different wavelengths in the fiber leads to pulse broadening [8]. Effects due to non-linearities in optical fiber increase for higher input signal powers and accumulate with the addition of each amplifier, distorting the optical bit-stream as the length of the optical path increases [9]. Four-wave mixing is a non-linear effect that becomes important for WDM systems [7]. These effects constrain the further increase in the capacity or bandwidth of the lightwave (optical) networks.

To accommodate future bandwidth requirements, advanced modulation schemes more spectrally efficient than conventional on-off keying are being explored, such as multi-level phase modulation, where the phase of the carrier is modulated with the spectrally efficient signal information [1]. Hence a channel analyzer capable of measuring close spectral features of a modulated signal spectra, the spectral purity of laser transmitters, and subtle changes such as spectral broadening due to non-linearities is necessary to test and analyze the performance of these advanced communication links.

A spectrum analyzer is an instrument used to study the properties of a signal by analyzing its spectral components. The following sections describe the evolution of various optical spectrum analyzers from grating based to high-resolution spectrum analyzers that include spectrum analyzers based on heterodyne detection and the most recent instrument based on the narrow gain profile of Stimulated Brillouin Scattering (SBS).

1.2 Grating Based Optical Spectrum Analyzers

Conventional optical spectrum analyzers (OSA) or spectrometers use a diffraction grating to disperse incoming light into different directions and a photo-detector array such as a charge-coupled device (CCD) array to measure the intensities of the spatially-separated wavelength components. Monochromators operate based on the same principle of dispersion as a spectrometer, however unlike a spectrometer, an exit slit is placed at the output, which selects a narrow range of wavelengths from a broader range available at the input. Figure 1shows the schematic of a common monochromator design: the Czerny-Turner monochromator.

The optical signal that is to be analyzed (A) is focused into a slit (B) using a lens and falls on the diffraction grating (D) after being collimated with a lens or mirror (C). The transmitted light is focused at the output slit (F) using another mirror or focussing lens (E). Due to diffraction of light incident on a surface with periodic variations in density or

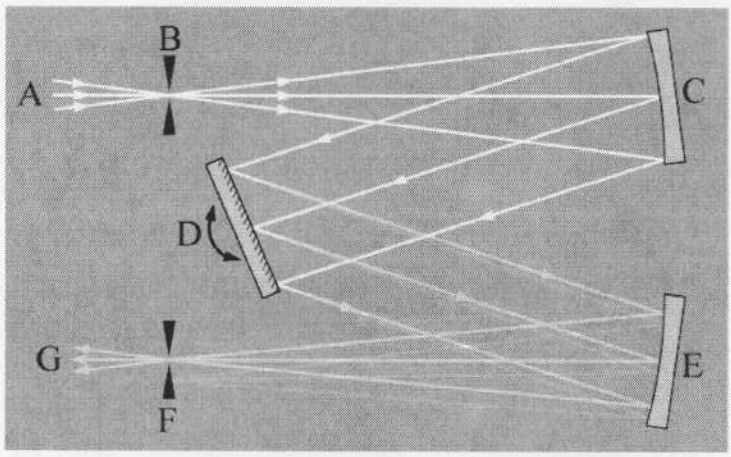

Figure 1. Schematic of a common Czerny-Turner monochromator
Figure borrowed from http://en.wikipedia.org/wiki/Monochromator

roughness, light of different wavelengths exit the diffraction grating at different angles depending on the periodicity of the structure. The mirrors can be mechanically rotated to scan and focus light of the desired wavelength onto the exit slit. The monochromator acts as an optical filter transmitting light of a certain wavelength. In a spectrometer, a CCD array is used instead of the exit slit to simultaneously measure the spatially-separated wavelength components of the light source being analyzed.

Although grating based OSAs have as wide tuning range (600 to 1700nm), they suffer from poor frequency resolution. The resolution bandwidth (often mentioned in nm) of the OSA is related to the focal length of the collimating lenses used. High-performance (in terms of wavelength resolution) grating-based OSAs are generally big and require exceptional mechanical and thermal stability. The best resolution bandwidth reported for

a conventional grating-based OSA by Agilent is 0.06nm [2]. This resolution bandwidth is a severe limitation in the application of conventional OSAs for measuring various close spectral features in a modern optical communication link, as mentioned in the previous section.

1.3 Heterodyne detection based High Resolution Optical Spectrum Analyzers (HRSA)

Heterodyne detection is a technique commonly used in radio-frequency spectrum analyzers (RF-SA). Figure 2 shows the operating principle of an optical spectrum analyzer based on heterodyne detection.

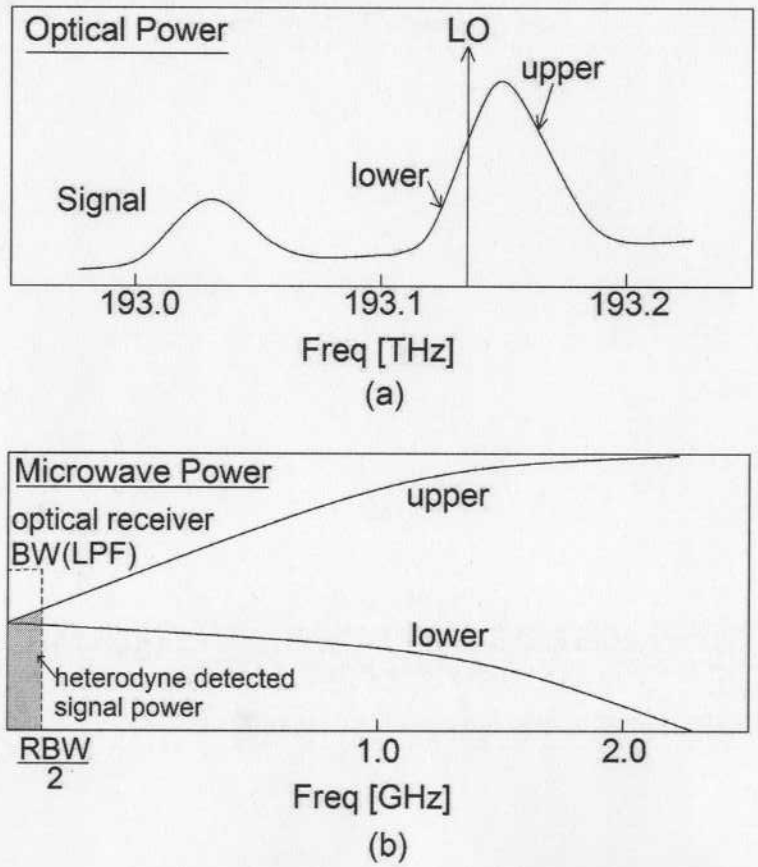

Figure 2. Principle behind the working of a heterodyne detection based optical spectrum analyzer: optical signal intensity is converted to the RF or Microwave frequency range and the down-converted signal is measured over the electrical bandwidth of the heterodyne receiver. Upper and lower denote frequencies above and below the LO frequency.

Heterodyne detection-based optical spectrum analyzers work on the same principle as a super-heterodyne radio receiver. A highly stable and tuneable signal with low phase noise is used as a local oscillator (LO). The LO frequency is tuned across the spectral range of interest of the input signal and is mixed with the signal in a non-linear device as shown in Figure.2a. Mixers are commonly used in heterodyne radio receivers to transfer RF signal power into intermediate frequencies (IF) for easier and inexpensive signal processing. Photodetectors are used to perform the corresponding non-linear operation in optical frequencies. The square-law intensity-to-photocurrent transfer function of a photodetector causes the non-linear mixing of the input optical signal with the LO. If the input signals are considered as two sinusoids, the output photocurrent comprises of the beat products which consist of the sum and difference frequency terms, and the direct-detected DC term with amplitude proportional to the total optical signal intensity at the input. The signal power is then determined by measuring the power of the frequency-downcoverted signal (in RF range for optically heterodyned signal) with amplitude at DC corresponding to the signal power at the LO frequency, as shown in Figure.2b. Resolution bandwidth (RBW) of the spectrum analyzer is determined by the bandwidth of the IF low-pass or band-pass filter in the optical receiver. Sections 2.0 and 3.0 describe the theory of balanced coherent detection and IF power detection.

Recently high-resolution spectrum analyzers (HRSAs) based on heterodyne detection have been built by Agilent and Apex technologies, with a resolution bandwidth limit of 12MHz over a tuning range of 200THz, covering the entire International Telecommunication (ITU) C and L-bands [5,6].

1.4 BOSA

More recently, Aragon Photonics Inc. built a high-resolution optical spectrum analyzer (BOSA) based on stimulated Brillouin scattering (SBS) [10]. SBS is a non-linear effect that occurs in optical fiber by which a portion of the power of a high-intensity incident wave (pump signal) is shifted to a narrow spectral region at a certain frequency offset, called the Doppler shift from the pump signal [11]. The scattered signal travels in the opposite direction of the incident wave and has a narrow bandwidth (roughly 10MHz). The Doppler shift is characteristic of the temperature and composition of the medium and is approximately 10.8GHz from a pump signal at 1550nm in a silica fiber at room temperature [12]. The narrow SBS gain bandwidth can be used to selectively amplify a very narrow portion of input signal spectrum and a high resolution spectrum can be obtained by tuning the pump signal frequency across the frequency range of input signal. Figure 3 shows the schematic of the BOSA.

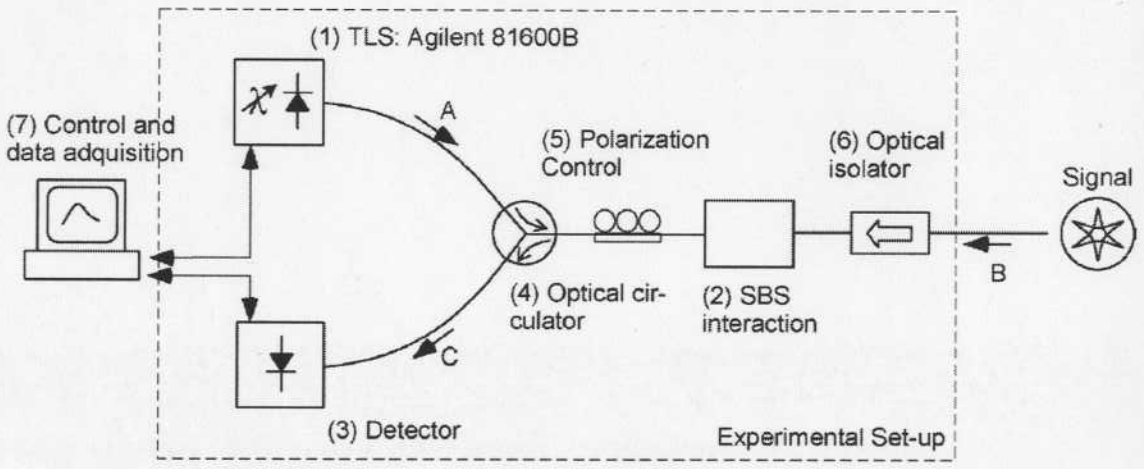

Figure 3. Schematic of the experimental setup of the BOSA. Signal under test (A) interacts with a strong pump signal (B) propagating in the opposite direction over a long length of fiber (2). The scattered signal (C) is selectively amplified over a narrow bandwidth (~10MHz) due to SBS phenomenon in an optical fiber and detected using a photo-detector (3).

Courtesy of [10]

A tunable light source (1) emits a high-intensity pump signal (A), which is made to interact with the optical signal of interest (B) over a long distance of optical fiber (~20km). Due to SBS, energy is transferred from the pump signal to a very narrow (10MHz bandwidth) portion of the incident signal close to 10.8GHz away from the pump signal center frequency. The signal at the end of the fiber thus contains the input signal with a narrow range of spectral components selectively amplified. An optical circulator is used to ensure the output signal (C) exits at a separate port and is isolated from the pump signal. The output signal intensity is directly detected using a photodetector and the frequency information is obtained from the control system used to tune the frequency of the tunable laser.

The optical spectrum analyzer (BOSA) built based on the technique described above is claimed to have a resolution bandwidth of 10MHz corresponding to the SBS gain bandwidth, and a dynamic range of 80dB over the wide tuning range of the ECT laser [10]. The BOSA employs a much simpler detection technique compared to that of HRSAs and the spectral measurements are not affected by the presence of the side-lobes commonly present in ECT lasers.

1.5 Coherent Channel Analyzer

Both the HRSA and the BOSA use a tunable-external cavity (ECT) diode lasers as the tunable light source. The narrow linewidth (typically 100 kHz) and broad tuning range of ECT lasers make them a good LO source. Wavelength tuning of a tunable ECT lasers is achieved by mechanically rotating a diffraction grating in the external resonator of the laser [13]. This makes them generally large and expensive. The high-resolution spectrum analyzer built by Agilent technologies (HRSA) sells for more than $150,000. In this

thesis we explore the use of a more compact and commercially used laser source, the distributed feedback (DFB) laser as a LO source to build a high resolution coherent channel analyzer (CCA). The use of a DFB laser as LO source can reduce the price of the instrument to a tenth of that of an HRSA.

DFB lasers are semiconductor lasers with the active region periodically structured as a diffraction grating which provides optical feedback for the laser, unlike typical laser designs that use mirrors to form the optical cavity [14]. The intensity and frequency of the emitted light can be controlled by adjusting the laser drive current and the temperature of the laser. DFB lasers have various commercial applications due to their small size which allows them to be packaged easily and controlled using temperature and current controllers. A key advantage of DFB lasers is the absence of sensitive opto-mechanical components used in ECT lasers. This makes them robust and easy to use while reducing their size and cost considerably [16].

One of the limitations of a DFB laser is its tuning range. Tuning of a DFB laser is accomplished by a change of the effective grating period by either electric (current) or thermal modulation. While a mechanical change of the resonator geometry allows the tuning of an ECT laser across a few tens of nanometers, the mode-hop-free temperature-tuning range of a DFB laser is limited to 3 to 4nm [16]. This can cover up to ten 50GHz spaced DWDM channels. Although this is much narrower compared to the total bandwidth of the C and L bands used in optical communication systems, various significant spectral features of interest for the analysis of a channel performance such as the modulation spectra, spectral broadening due to non-linearities and dispersion effects and the laser transmission spectra can be studied using a carrier centered in the 1550nm

range. The use of a DFB laser as a LO offers tremendous cost (ten times) and size (5 times) advantage compared to ECT lasers, while providing comparable frequency resolution. The potential cost and size advantage of the CCA may far outweigh the inconvenience of having to study the spectra at a certain carrier wavelength range.

Another limitation of DFB lasers is its broad linewidth (10-100 times that of ECT lasers) with a long Lorentzian tail due to spontaneous emission in the optical gain process [15]. An ideal LO has zero linewidth and zero frequency jitter, in which case the resolution of the spectrum analyzer is limited purely by the optical receiver bandwidth or RF output low-pass filter. The linewidth of the DFB laser used in the CCA and the loss in sensitivity and spectral resolution due to the LO phase noise is characterized in section 5.

In this thesis we provide the theoretical analysis for the signal and noise power in heterodyne detection and the SNR model for the CCA. The end-to-end system model of the CCA, predicting the detected signal power for a given input optical signal intensity is also shown. The properties of various system components such as the phase noise of the LO and the transfer function and output noise of the RF power detector are studied and verified experimentally. Experimental results are shown to match the theoretically predicted values from the system model. We demonstrate a frequency resolution of 100MHz over the tuning range of the DFB laser (close to 200GHz) with a sensitivity of -95dBm and a 100Hz detection (video) bandwidth (VBW).

2.0 Theory

Heterodyne detection refers to the method of detecting a signal by non-linear mixing with a reference signal (LO). Non-linear devices such as diodes for RF-signals and photo-diodes for optical signals have a non-linear transfer characteristic with respect to amplitude and generate an output signal proportional to square of the input signal-amplitude. In the simplest case of two single-tone signals at the input, the output signal includes a component at the difference frequency, with amplitude and phase related to that of the input signal.

When the LO frequency is close to the signal frequency of interest, the heterodyne signal is down-converted to a frequency where signal processing is easier. This is one of the advantages of heterodyne-detection, and is the principle used in spectral analysis in a coherent optical spectrum or channel analyzer. Since the power or intensity of the heterodyne-detected signal is a product of the signal and LO signal intensities, this method is also more sensitive than direct-detection of weak signals.

Information on phase of the input signal can be obtained from the heterodyne-detected signal if the phase of the LO is known. For this reason, a coherent source with a stable phase is important for measurements involving the phase of the input signal. Hence, this method is also called coherent detection.

One of the major noise sources in optical coherent detection is the intensity noise (RIN) of the LO. Balanced coherent detection is a slightly modified detection scheme that has been shown to be effective in RIN suppression [17, 18].The next section describes the theory of balanced coherent detection.

2.1 Balanced Coherent Detection

A schematic of coherent detection of a signal using a balanced-optical receiver is shown in Figure 4.

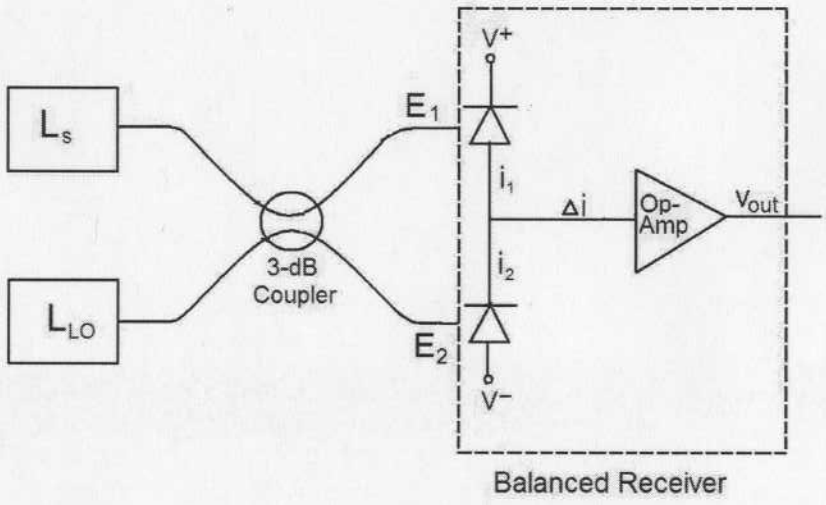

Figure 4. Schematic of an optical balanced heterodyne receiver

In this section we derive the output signal power of a balanced-coherent receiver. This is not a new result, but will aid the explanation of new results to be presented later. The signal under test considered in this derivation is an intensity-modulated signal. The equation for the electric field of the signal under test at a frequency ω_s, with intensity modulation $m(t)$, and a time-varying phase $\Phi_s(t)$ can be represented as

$$L_s = E_s\left[1 + m(t)\right]^{1/2} \exp\left[-j\left(\omega_s t + \Phi_s(t)\right)\right] \ . \tag{1}$$

Similarly the local oscillator field at a frequency ω_{LO}, is given by

$$L_{LO} = E_{LO}\left[1 + a(t)\right]^{1/2} \exp\left[-j\left(\omega_{LO} t + \Phi_{LO}(t)\right)\right] . \tag{2}$$

The random intensity and phase fluctuations of the LO given by $a(t)$ and $\Phi_{LO}(t)$, respectively, contribute to the intensity and phase noise of the LO. The contribution of LO intensity and phase noise in the detected output signal is analyzed in section 3.0.

The optical signal and the LO are coupled together in a 3-dB coupler, which introduces a 90° phase difference in the electric field of the two output branches. The two output branches of the coupler are fed into a balanced-optical receiver. Assuming an ideal 3-dB coupler and that the polarizations of the two inputs are matched using polarization controllers (see

Figure 10 for the experimental setup of the CCA) the total field in the two output ports of the coupler is given by

$$E_1 = \frac{1}{\sqrt{2}}\left\{E_s\sqrt{1+m(t)}e^{-j(\omega_s t+\Theta_s(t))} + E_{LO}\sqrt{1+a(t)}\; e^{-j\left(\omega_{LO}t+\Theta_{LO}(t)+\pi/2\right)}\right\} \qquad (3)$$

and,

$$E_2 = \frac{1}{\sqrt{2}}\left\{E_s\sqrt{1+m(t)}e^{-j\left(\omega_s t+\Theta_s(t)+\pi/2\right)} + E_{LO}\sqrt{1+a(t)}\; e^{-j(\omega_{LO}t+\Theta_{LO}(t))}\right\}. \qquad (4)$$

Assuming the responsivity of the photodetectors to be $1\,A/W$, the photocurrent generated in the two photodiodes is given by

$$i_1 = i_s(1+m(t)) + i_{LO}(1+a(t)) - 2\sqrt{i_s i_{LO}}\sqrt{1+m(t)}\sqrt{1+a(t)}\sin[(\Delta\omega)t + \Delta\Phi(t)] \qquad (5)$$

and,

$$i_2 = i_s(1+m(t)) + i_{LO}(1+a(t)) + 2\sqrt{i_s i_{LO}}\sqrt{1+m(t)}\sqrt{1+a(t)}\sin[(\Delta\omega)t + \Delta\Phi(t)] \quad , \qquad (6)$$

where,

$\Delta\omega = \omega_s - \omega_{LO}$, and

$\Delta\Phi(t) = \Phi_s(t) - \Phi_{LO}(t)$.

The currents from the two branches are subtracted in the balanced receiver. If the two branches are perfectly balanced, the direct-detected current in each branch is equal and will be cancelled, whereas the cross product terms are out of phase and add. The signal at the output is a sinusoid at the difference frequency with twice the amplitude of the cross-product terms in the individual branches:

$$\Delta i = 4\sqrt{i_s i_{LO}}\sqrt{1+m(t)}\sqrt{1+a(t)}\sin\left[(\Delta\omega)t + \Delta\Phi(t)\right] . \qquad (7)$$

From the above expression, it is clear that the amplitude and phase of the output photocurrent (Δi) have random fluctuations arising from the intensity and phase noise of the LO. In Section 3.1 the power spectral density of the output current is derived, which shows that the relative-intensity noise is small and can be neglected compared to the intensity-converted phase noise at frequencies close to the optical central frequency of the LO. The impact of the LO phase noise on the sensitivity and frequency resolution capability of the CCA is described in section 7.2.

The average signal power within the bandwidth of the optical receiver is found from the mean square value of the expression in eqn. (7):

$$\left\langle \Delta i^2 \right\rangle = 8 i_s i_{LO}\left(1 + m(t)\right) \qquad (8)$$

The local-oscillator is swept across the frequency range of the input signal and the RF power within the optical receiver bandwidth, given by eqn. (8), is detected with an RF power detector.

2.2 Noise Sources in Coherent Detection

The major noise sources at the output of the balanced-optical receiver are thermal noise of the balanced receiver, shot noise from the random arrival of photons at each of the photo detectors and relative intensity noise (RIN) from the intensity fluctuations of the

local oscillator [19]. Expressions for the variances of each of the noise current are explained in this section.

Thermal noise current variance of a receiver with an amplifier noise figure F_n, load resistance R_L and temperature T is given by [20, 21]

$$\sigma_T^2 = \frac{4k_B T F_n}{R_L} \qquad A^2/Hz \quad , \tag{9}$$

where k_B is Boltzmann's constant. Thermal noise is the dominant noise source in most practical receivers at low input optical power levels. High impedance or trans-impedance amplifiers can be used to reduce thermal noise. The effect of thermal noise is often quantified by the manufacturer in terms of noise-equivalent power (NEP). NEP is defined as the minimum input power per unit bandwidth that results in an output SNR of 1. Typical NEP values for an optical receiver with a trans-impedance amplifier are in the range of $1-10\ ^{pW}/_{\sqrt{Hz}}$ or of the order of $10^{-23}\ ^{A^2}/_{Hz}$, assuming responsivity of $1\ ^{A}/_{W}$ [19].

Shot noise from the sum of the direct-detected current terms $i_1 + i_2$ from the two photodetectors is given by [22]

$$\sigma_s^2 = 2e(i_1 + i_2) \quad A^2/Hz \quad , \tag{10}$$

where e is the charge of an electron $1.6\times10^{-19}C$. For an LO intensity much greater than the signal, i.e. $i_{LO} >> i_s$ the total current $(i_1 + i_2)$ can be approximated as $2i_{LO}$. For a LO with intensity 0dBm, the variance in the shot-noise current is $6.4\times10^{-22}\ ^{A^2}/_{Hz}$.

The power spectral density (PSD) expression for the relative intensity noise (RIN) of a laser can be derived from the rate equations [23]. It has been shown to be a function of frequency and laser power. At a given laser power, RIN has a peak value in the vicinity

of the resonance frequency (Ω_R) and is relatively low when $\omega << \Omega_R$. Typical value of *RIN* for most DFB lasers is -150 dB/Hz. The resulting intensity noise current variance is given by

$$\sigma_I^2 = (i_1 + i_2)^2 \, RIN \quad A^2/Hz \quad . \tag{11}$$

For a strong LO power, RIN can be the predominant noise source for coherent detection without a balanced receiver. The common-mode signals in the two branches of a balanced receiver, including the intensity noise of the LO, are suppressed by the common-mode rejection ratio (CMRR) value specified for the balanced receiver. Effective RIN suppression for a well-balanced receiver where the total intensity in the two optical paths is matched can thus increase the dynamic range of the system. Using eqn. (11), the RIN current variance for a LO with intensity 0dBm and a CMRR value of 25dB in a perfectly balanced receiver is $\sim 3 \times 10^{-24}$ A^2/Hz.

The SNR at the output of the receiver with a bandwidth B can thus be expressed as

$$SNR = \frac{\langle \Delta i^2 \rangle}{(\sigma_T^2 + \sigma_S^2 + \sigma_I^2)B} \quad , \tag{12}$$

where the signal contribution comes from the total signal power within the receiver bandwidth B.

As shown in eqn. (8), the detected signal is proportional to the LO power. Thermal noise is independent of the photo-detected current while shot noise varies linearly with the photo-detected current from the signal and LO. For an ideal system with perfect RIN suppression, maximum SNR can be achieved by increasing the LO intensity until shot noise is the dominant noise source. Figure 18 in section 6.1 shows the signal and total

noise power versus LO intensity for the CCA, from which it can be seen that the maximum SNR of the system is achieved for an LO power between 0 and 15dBm , when the noise power is dominated by the shot noise. Since shot noise increases linearly with the LO intensity, further increase in LO power does not improve the SNR of the system.

2.3 Video Noise

The ability to observe a weak signal in the presence of additive white noise determines the sensitivity of the system. The last stage of the CCA is an RF power-detector which measures the heterodyne signal and noise power at the output of the balanced-optical receiver. Derivation of the output SNR of the CCA involves characterization of the noise at the output of the RF-power detector, called video noise. The noise is termed video-noise keeping with historical convention of the terminology for signals at the output of an RF detector. In this section, we determine the video noise spectral density or the variance of the output of the RF-power detector with a bandlimited Gaussian white noise as the input signal.

The RF power detector can be modelled as a squaring device (square-law detector) followed by an integrator or low pass filter, as shown in Figure 5.

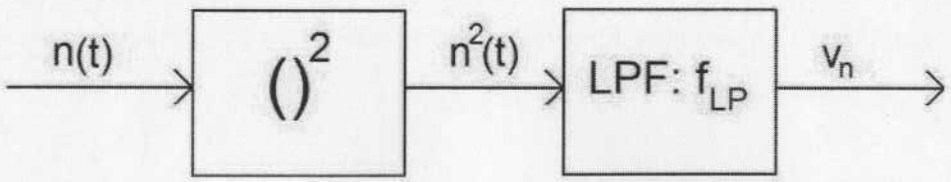

Figure 5. Block Diagram of the components of a square-law RF power-detector

The DC output voltage, $\langle v_n \rangle$ of the power-detector is directly proportional to the input RF signal power or input band-limited noise power. If the input of the power detector $n(t)$ is band-limited noise, the output $\left(n^2(t)\right)$ of the square-law detector is also a bandlimited signal with a spectral distribution. The low-pass filter at the output of the square-law detector defines the video bandwidth, f_{LP}. The total noise-power within the video bandwidth (VBW) at the output of the square-law detector determines the variance of the DC output $\left(\langle v_n \rangle\right)$ of the RF power detector.

The rms fluctuations of the output voltage of the power detector is given by,

$$\sigma_n = \sqrt{\langle v_n^2 \rangle - \langle v_n \rangle^2}\,, \tag{13}$$

where v_n represents the instantaneous output voltage. The bandwidth of the input RF bandlimited noise is B. The low-pass filter can be considered as an averaging device which reduces the variance by the ratio of the bandwidth of the input RF noise signal, B and the low-pass filter bandwidth, f_{LP}. Mathematically, assuming a flat noise PSD at the input of the detector, it can be expressed as [24],

$$\sigma_n = \frac{\sigma}{\sqrt{B/f_{LP}}}\,, \tag{14}$$

where σ is the standard deviation of the output, $n^2(t)$ of the square-law detector. For an input $n(t)$, which is a noise voltage obeying a Gaussian statistical distribution, the standard deviation σ of the output of the square-law detector, is equal to the mean value of the output of the square-law detector [24]. That is,

$$\sigma = \langle n^2(t) \rangle = \langle v_n \rangle . \tag{15}$$

From Eqns (14) and (15), it is clear that for a band-limited RF noise signal at the input, the variance of the detected noise at the output reduces with the bandwidth of the low-pass filter of the power detector, or equivalently, by using a longer averaging time. However this would lead to a slower read-out time. The time taken by the CCA to measure a spectrum is proportional to the frequency range being measured and inversely proportional to both the resolution bandwidth and video bandwidth.

3.0 Impact of LO Phase and Intensity noise

One of the requirements of coherent detection is a strong LO source with a stable intensity and phase since the LO is used as a reference from which the signal information is obtained. Thus random fluctuations in the LO intensity and phase, characterized by the intensity and phase noise, respectively, appear as intensity noise in heterodyne-detected signal and can limit the sensitivity of the detection. In this section, we derive the power-spectral-density (PSD) of the signal at the output of a balanced-coherent receiver which shows the contribution of the LO- phase and intensity noise in a coherent-detected signal. From this expression, we derive the CCA-measured output spectrum of a continuous-wave (CW) signal and explain the spectral broadening due to the LO phase noise.

3.1 Heterodyne Conversion of Optical Noise

Spontaneous emission in the laser leads to random intensity and phase fluctuations in the laser output [23]. In this section we derive an expression for the PSD of the current signal generated in the balanced-coherent receiver assuming perfect RIN suppression, which describes the contribution of the LO intensity and phase noise in heterodyne detection.

In section 2.1, an expression (eqn. (7)) for the current at the output of a balanced-coherent receiver was derived for an intensity-modulated input optical signal. Considering the scenario where modulation is turned off ($m(t) = 0$), the heterodyne detected current signal in a perfectly balanced-coherent receiver (ideal RIN suppression) can be expressed as:

$$\Delta i(t) = 4\sqrt{i_s i_{LO}}\sqrt{1+a_1(t)}\sqrt{1+a_2(t)}\cos\left[(\Delta\omega)t + \Delta\phi(t) - \pi/2\right] \quad , \qquad (16)$$

where $a_1(t)$ and $a_2(t)$ represent the intensity fluctuations of the two beating lasers and can be modeled as zero-mean Gaussian stochastic random processes [23]. The fluctuations in the phase of a laser, like the intensity, can also be modeled as a zero-mean Gaussian stochastic random process [26]. Since the two signals are derived from independent laser sources, their phase is uncorrelated and the instantaneous phase difference $(\Delta\phi(t))$ of the two signals can be considered to have the same statistical properties as the phase of the individual signals. i_s and i_{LO} represents the 3-dB intensities of the signal and LO lasers, respectively, and $\Delta\omega$ represents the frequency difference between the center frequencies of the two lasers.

Autocorrelation of the heterodyne current signal in the balanced receiver $(\Delta i(t))$ is defined as,

$$R_{II}(\tau) = \left\langle \Delta i(t)\Delta i^*(t+\tau) \right\rangle, \tag{17}$$

where $\Delta i^*(t)$ represents the complex conjugate, $\langle\rangle$ represents the ensemble average, and τ denotes a time offset. Using eqn. (16) to expand the above expression and noting that since the ensemble average is equal to the time average for a Gaussian random process, all the terms with an explicit $e^{j\omega t}$ dependence average out to 0 and the signal autocorrelation can be expressed as [27]

$$\begin{aligned} R_{II}(\tau) = 4i_s i_{LO} \langle\ & \sqrt{(1+a_1(t))(1+a_2(t)).(1+a_1(t+\tau))(1+a_2(t+\tau))} \\ & \exp j(\Delta\omega\tau + \Delta\phi_2(t,\tau) - \Delta\phi_1(t,\tau)) + CC\ \rangle, \end{aligned} \tag{18}$$

where $\Delta\phi_{1,2}(t,\tau) = \phi_{1,2}(t+\tau) - \phi_{1,2}(t)$ is the difference between the instantaneous phase of the laser and a time-shifted version of itself. CC represents the complex conjugate of the previous term. $a_1(t)$ and $a_2(t)$ are uncorrelated Gaussian random variables with a mean

value of 0, such that $\langle a_1(t)\rangle = \langle a_2(t)\rangle = \langle a_1(t)a_2(t+\tau\rangle = \langle a_1(t+\tau)a_2(t)\rangle = 0$ and the contribution from the higher-order terms can be neglected. Using the relationship from [28],

$$\left\langle \exp\left(j\Delta\phi_{1,2}(t,\tau)\right)\right\rangle = \exp\left(-|\tau|/\tau_{c1,2}\right) \tag{19}$$

where $\tau_{c1,2}$ denotes the coherence times of the lasers, Eq. (18) can then be expressed as:

$$R_{II}(\tau) = 4i_s i_{LO}\left[\ (e^{j\Delta\omega\tau} + e^{-j\Delta\omega\tau})\exp\left(-|\tau|/\tau'\right)\ \right]\left\{1+\frac{1}{2}(R_{A1}(\tau)+R_{A2}(\tau))\right\}. \tag{20}$$

$R(\tau)$ is the intensity autocorrelation function defined as $R_A(\tau) = \langle a(t)a(t+\tau)\rangle$, and $1/\tau' = 1/\tau_{c1} + 1/\tau_{c2}$. Considering the most common scenario where the two lasers have the same intensity noise distribution, i.e. $R_{A1}(\tau) = R_{A2}(\tau) = R_A(\tau)$, Eq. (20) reduces to

$$R_{II}(\tau) = 4i_s i_{LO}\left[2\cos(\Delta\omega\tau)e^{-|\tau|/\tau'}\left(1+R_A(\tau)\right)\right] \tag{21}$$

Intensity noise of a DFB lasers is characterized by the relative intensity noise (RIN) with a typical value of -150 dB/Hz [23]. The term $R_A(\tau).\exp\left(-|\tau|/\tau'\right)$ represents the convolution between phase and intensity noise in the frequency domain, which can be neglected compared to the other term in the bracket representing phase noise for frequencies close to the optical center frequency of the laser. Fourier transform of the remaining terms in Eq. (21) yields the two-sided power spectral density of the detected signal as

$$I(\Omega) = 4i_s i_{LO}[\phi(\Omega-\Delta\Omega)+\phi(\Omega+\Delta\Omega)], \tag{22}$$

where
$$\phi(\Omega) = \frac{1}{\Omega_0} \frac{1}{1 + \left(\Omega / \Omega_0\right)^2} \tag{23}$$

describes the Lorentzian shape of the spectrum with a FWHM linewidth of $2\Omega_0 = 2\pi/\tau$, which is equal to the twice the sum of the linewidths of the two lasers. For an ideal LO and laser signal, each with zero-linewidth $(\Omega_0 = 0)$, the spectrum would reduce to a delta-function at frequency $\Delta\omega$.

From Eq. (22) and (23), it is clear that the PSD of the detected signal current is spread due to the phase noise of the lasers and has a Lorentzian shape. Integration over the bandwidth of the signal results in the same signal power as expressed by eqn. (8). Figure 6 shows the PSD of the detected current, normalized with respect to the total signal power $(8 i_s i_{LO})$, for different values of the sum of the laser linewidths. The RIN spectrum is considered to be white with a magnitude of $-150 dB/Hz$, and is shown in Figure 6 as the horizontal straight line at bottom. It can be seen that RIN can generally be ignored in comparison to the converted phase noise for the frequency range (close to DC) within the bandwidth of the receiver. From the figure we see that the bandwidth of the converted phase noise is equal to the sum of the laser linewidths. The signal (CW laser signal with zero linewidth) power detected with the use of a zero linewidth LO laser is shown in Figure 6 as the delta function (red arrowed line) at DC. From the analysis presented here, it is clear that the signal current generated in the balanced receiver is spread across a broad spectrum, which along with the frequency jitter on the LO sets the lower-limit on the RBW of the CCA.

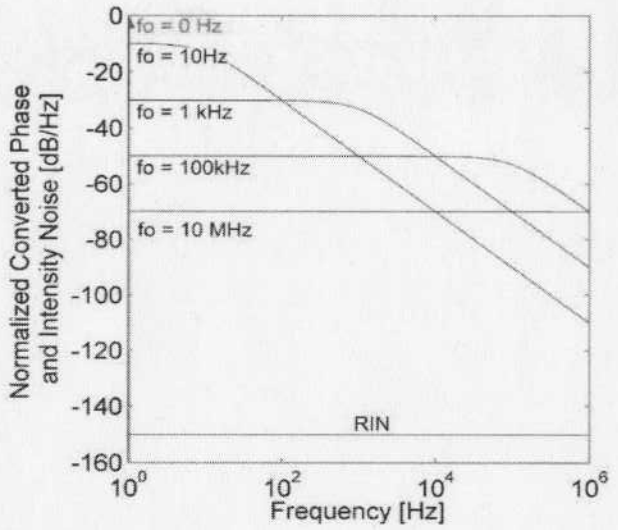

Figure 6. Normalized intensity and converted phase noise spectrum for different values of laser linewidths based on equations (22) and (23).

3.2 Output Spectrum Characterization for Converted LO Phase Noise

In the previous section, the impact of the LO laser linewidth on the bandwidth of the output signal of a balanced-coherent receiver was analyzed. Current high-resolution optical spectrum analyzers (HRSAs) use large and expensive external cavity (ECT) lasers as the LO with a typical linewidth of ~100kHz [5]. Figure 7 compares the spectral measurement of a CW ECT laser signal using the CCA with (a) an ECT laser and (b) a temperature-tuned DFB laser as LO.

One of the limitations of a DFB laser is its broad Lorentzian shaped field spectrum due to the laser phase noise. The measured output spectrum in Figure 7(b) shows the spectral broadening caused by the converted phase noise of the DFB laser. From Figure 7(a), the noise floor at a frequency offset 80MHz away from the central frequency is dominated by the receiver noise, whereas in Figure 7(b), the Lorentzian tail of the DFB LO laser is visible up to 4GHz from the center frequency of the signal. In this section we characterize the intensity-converted phase noise floor at the output of the CCA.

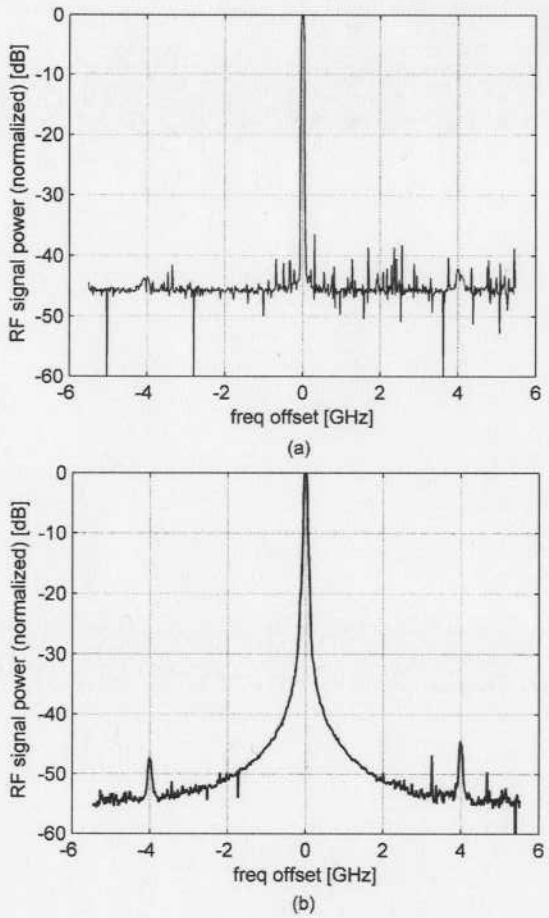

Figure 7. Spectrum of an ECT laser measured using the CCA with (a) an ECT laser as LO and (b) DFB laser as LO.

From the analysis in section 3.1 (equations (22) and (23)), the single-sided PSD of the signal at the output of the balanced-coherent receiver is given by

$$S(\omega) = 8 i_s i_{LO} \frac{2/\tau_c}{\left(1/\tau_c\right)^2 + \omega^2} \quad , \tag{24}$$

where τ_c is the coherence time of the LO (DFB laser for the CCA), which determines the DFB laser linewidth. Expressing the PSD in units of per Hertz, eqn. (24) becomes

$$S(f)=\frac{2P_o}{\pi B_o}\frac{1}{1+\left(\frac{(f-f_o)}{B_o/2}\right)^2} \quad \left[A^2/Hz\right] \quad , \qquad (25)$$

where $B_o = 1/\pi\tau_c$ is the FWHM bandwidth of the Lorentzian-shaped signal spectrum, $P_o = 8i_s i_{LO}$ is the total signal power as derived in section 2.1, and f_o is the center frequency of the heterodyne-detected signal, which is the difference between the optical signal frequency and the DFB-laser (LO) center-frequency.

The CCA measures and displays the RF power within the optical receiver bandwidth as the local oscillator scans the input optical signal spectrum. This operation can be mathematically modelled as the convolution of the RF signal expressed in eqn. (25) with the transfer function of the low-pass filter of the balanced-optical receiver.

Assuming an ideal low-pass filter, the two-sided output spectrum measured by the CCA is given by

$$\begin{aligned} S_{CCA}(f) &= S(f) * H(f) \\ &= \frac{P_0}{\pi}\left\{\tan^{-1}\left(\frac{(f'+f_1)}{B_o/2}\right) - \tan^{-1}\left(\frac{(f'-f_1)}{B_o/2}\right)\right\}, \end{aligned} \qquad (26)$$

where $H(f)$ is the transfer function of an ideal low-pass filter with a cut-off frequency f_1 and $f' = f - f_o$ represents a change in variable with respect to the signal center frequency. The FWHM bandwidth (B_0) of the Lorentzian spectral profile of the DFB-laser optical field spectrum, and hence the heterodyne-detected signal, was measured experimentally to be 1.6MHz using delayed self-heterodyne detection as described in section 5.1. Validity of the model expressed by eqn (26) and that of the calibrated DFB

laser linewidth can be seen in Figure 8 which shows excellent agreement between the measured output spectrum of an ECT laser measured using the CCA with a resolution bandwidth of 50MHz and the theoretical model. The jitter of the DFB laser (LO) is in the range of 10-15MHz, which causes an increase in linewidth. This was taken into account in the model by increasing the pass band $(2f_1)$ of the receiver low-pass filter by 10MHz.

Figure 9 shows the increase in the CCA-measured LO phase-noise floor with the optical receiver bandwidth $(2f_1)$. The curves are based on eqn (26), normalized with respect to the signal power, and the optical receiver bandwidth values of to 50, 10, and 1MHz were used.

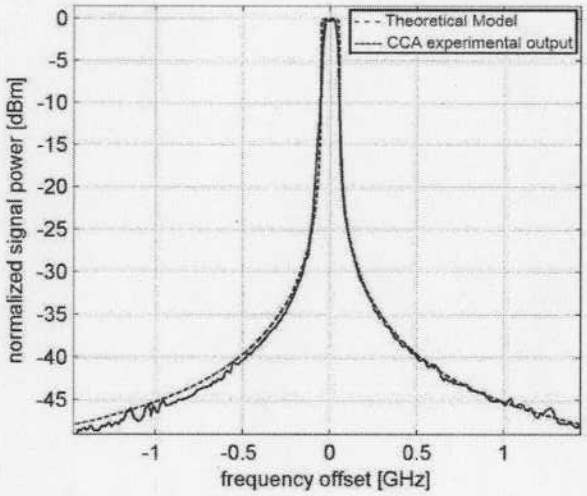

Figure 8. Theoretical model and experimental output of an ECT laser spectrum measured using the CCA.

As expected, the output noise is directly proportional to the measurement bandwidth. As a result, a 10dB and 7dB rise in the noise floor can be seen corresponding to a 10 times and 5 times increase in the optical receiver bandwidth respectively. The lower limit of the

resolution bandwidth of the CCA is limited by the 10-15MHz frequency-jitter of the DFB laser.

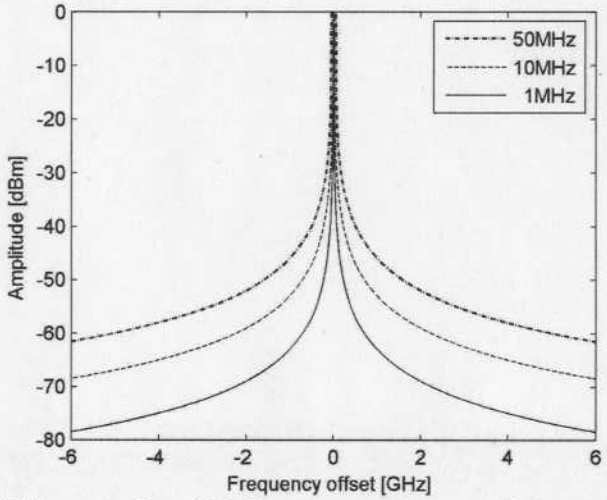

Figure 9. Theoretical model showing the impact of the optical receiver bandwidth on the measured phase noise at the CCA output, normalized to the heterodyne-detected signal power.

The theoretical curve given by eqn.(26) can be used to characterize the measured phase-noise floor at the output of the CCA. Due to the long Lorentzian tail of the DFB laser, the noise floor close to a strong-measured signal is dominated by phase noise and can limit the detectability of weak features in close proximity. For instance, weak sidebands can be buried in the LO phase noise with the detection of a strong carrier in the case of a phase-modulated signal, as demonstrated in section 7.2.

4.0 Experiment

The experimental setup of the CCA is shown in figure 10.

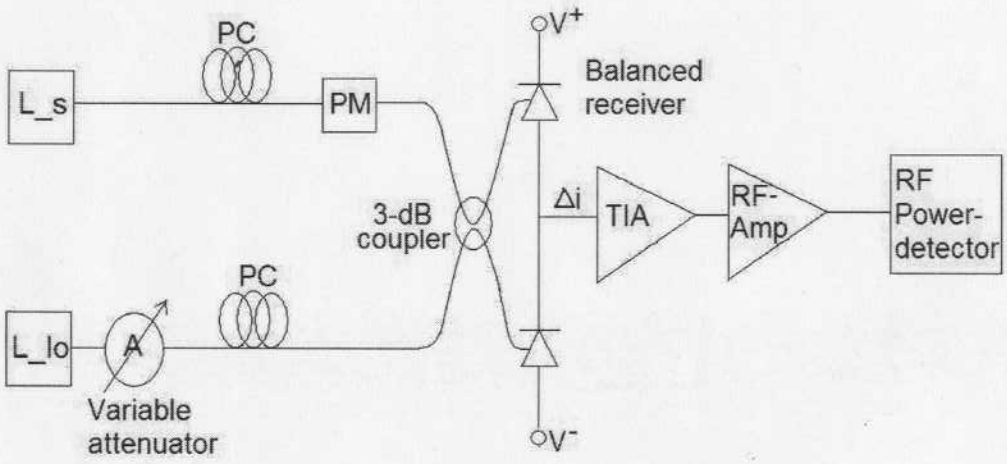

Figure 10. Schematic of the CCA

A temperature-tuned DFB laser (L_lo) was used as the local-oscillator. A variable optical attenuator controls the LO power to ensure the RF signal power is maintained within the dynamic range of the power detector. For the purpose of experimentation, the spectrum of a high-performance Agilent ECT laser (L_s) was measured. An electro-optic phase modulator (PM) was used to modulate the phase of the signal with a sinusoidal function, adding modulation sidebands with which the frequency sideband resolution limit of the CCA was tested. The input optical signal is coupled with the LO using a 3-dB coupler. Polarization controllers can be used in either of the input branches being fed into the coupler to ensure that polarizations of the two optical fields are aligned for maximum output signal power.

The 3-dB optical coupler combines and distributes the signal and LO fields into two output branches, which are fed into the two input ports of a Thorlabs PDB150C balanced receiver with adjustable RF gain and bandwidth. The balanced receiver has two DC output ports (see Figure 13) that can be used to measure the total optical intensity at each of the photodiodes and ensure balanced operation of the receiver. The heterodyne detected signal (Δi) obtained by subtracting the photocurrents generated in the two photodiodes is available at the RF output port of the balanced receiver.

An AD8362 RF power detector at the output of the balanced-optical receiver measures the RF signal power. The AD8362 is a true-rms integrated power detector that outputs a DC voltage proportional to the input logarithmic RF power. The amplifier at the output of the balanced receiver was used to ensure the signal is within the measurement dynamic range of the power detector. The low-pass filter bandwidth of the multi-meter used to measure the output voltage of the power detector determines the video bandwidth (VBW) of the CCA.

Calibration and characterization of the system components, including the balanced-optical receiver, true-rms power detector and the DFB laser LO linewidth, are described in the next section. These system component characteristics will be used to create the end-to-end system model of the CCA in section 6.0, with experimental data in section 7.0.

5.0 Characterization of system components

5.1 DFB laser linewidth

From the analysis shown in section 3.0, the noise power spectrum from the intensity-converted phase noise of the LO can be fully derived from the laser linewidth for a semiconductor LO laser with a Lorentzian field spectrum. This section describes the experimental characterization of the DFB LO laser linewidth used in the CCA.

Self-homodyne detection is a well established technique used to measure the laser field spectrum with high resolution [25]. It is based on the principle of coherent detection discussed in the section 2.0, by which phase information of the signal is converted into intensity using a Mach-Zehnder type interferometer and the spectrum of the photocurrent generated at the output of a high-speed photodetector is measured using an RF spectrum-analyzer. Fig. 12 shows the schematic of a self-homodyne detection setup used to measure the linewidth of a laser.

The laser field is split and fed into the two branches of the interferometer. A delay is introduced in one of the paths so that the phase of the two fields at the output is no longer correlated. Correlation analysis similar to that shown in section 3.1 for the combined field at the output can be used to obtain the intensity-converted phase-noise spectrum at the output [29]. If the path delay is longer than the laser phase coherence length, the two fields at the output of the interferometer become totally uncorrelated and simplify the intensity correlation analysis. The intensity spectrum of the combined signal consists of the sum of the input signal powers, intensity noise of the laser and the intensity-converted phase noise of the laser centered at DC [29]. For a Lorentzian field spectrum, as in the case of a semiconductor diode laser, the 3dB spectral spread then becomes twice the

value of that of the individual fields [25, 29]. A high-speed photodetector converts the intensity of the combined field to current and the photocurrent spectral density is measured using an FFT-based spectrum analyzer or dc-coupled RF Spectrum Analyzer. If the field in one of the branches is modulated using an acousto-optic modulator, the center frequency of the intensity-converted phase noise is shifted to a higher frequency which can be analyzed using a standard RF spectrum analyzer. This method is called self-heterodyne detection.

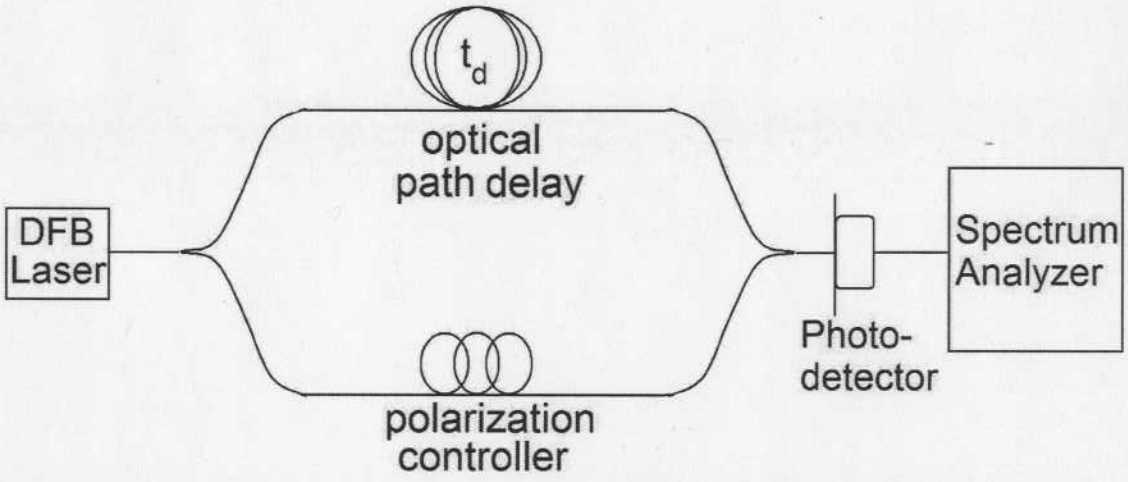

Figure 11. Schematic of experimental setup for DFB laser linewidth characterization using self-homodyne detection

Figure 12 shows the output photocurrent spectrum (solid line) of the self-homodyne detected signal using a dc-coupled Agilent E4440A RF spectrum analyzer. The laser examined was a 1.55 μm temperature-tuned Nortel DFB laser with a 35mA injection current and maintained at 34^0C. A 20km single-mode fiber loop was used to create a delay path much longer than the coherence length of the DFB laser. Bandwidth of optical receiver was set to 150MHz. The dashed line shows the Lorentzian curve fit with a 3-dB bandwidth of 3.2MHz. Good agreement between the curves can be seen until the receiver

noise begins to dominate from 50MHz to the receiver bandwidth of 150MHz. Thus the DFB laser has 3-dB optical-field spectral bandwidth (FWHM) or a laser-linewidth of 1.6MHz. This value was used to characterize the CCA output spectrum, which showed good agreement with the theoretical curve in fig. 8.

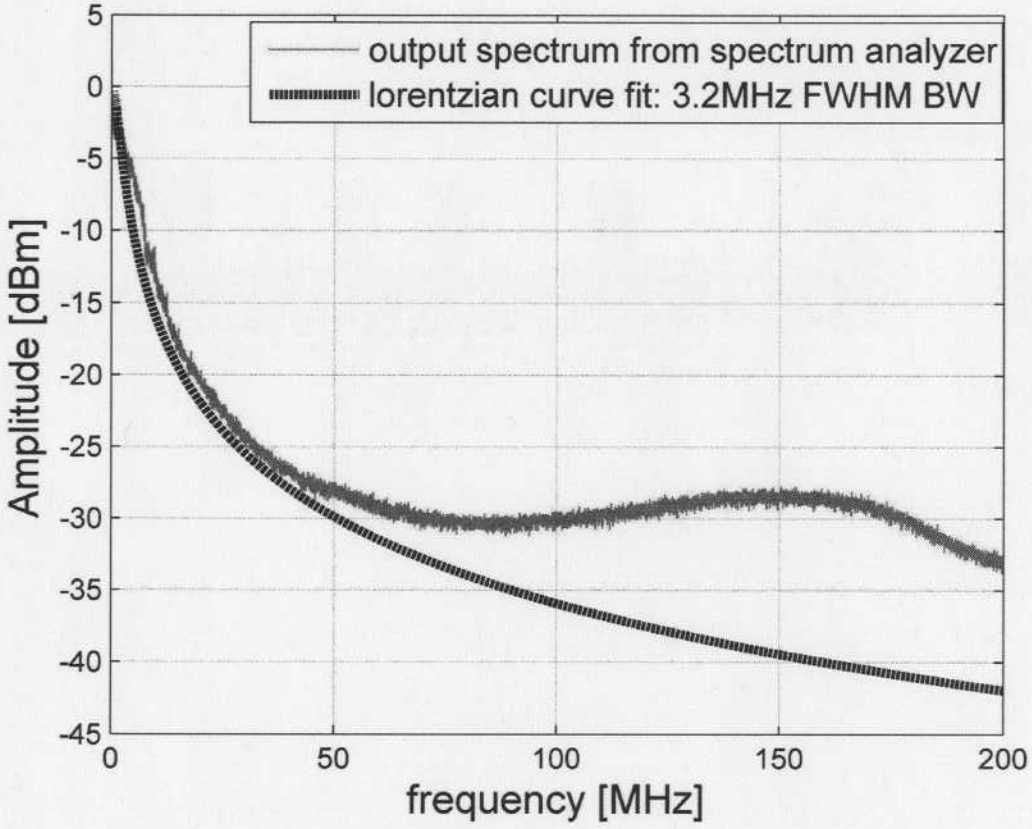

Figure 12. Spectral trace for DFB laser linewidth characterization.
Trace of the spectrum (red solid line) of the self-homodyne detection output signal from an Agilent E4440A RF spectrum analyzer with DC-coupling (capable of measuring from 3Hz) and RBW setting of 1Hz. Dotted line shows the Lorentzian curve fit with a FWHM bandwidth of 3.2MHz which is twice the DFB field spectral linewidth.

5.2 Balanced-Optical Receiver

One of the important components of a coherent system is the receiver. The design of the balanced-coherent receiver used in the CCA has a major impact on the frequency

resolution and sensitivity of the instrument. This section describes the design and important characteristics such as CMRR, receiver gain, bandwidth and noise characteristics of the Thorlabs PDB-150C balanced receiver used in the experiment.

A schematic of the Thorlabs PDB-150C balanced-optical receiver is shown in Figure 13.

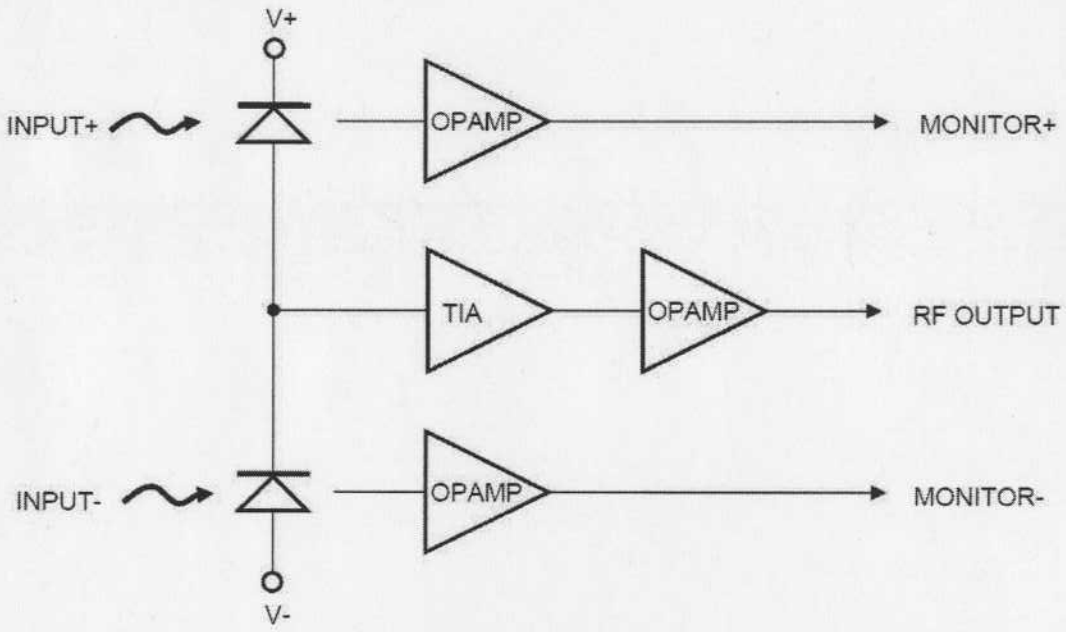

Figure 13. Schematic of the Thorlabs PDB-150C balanced-optical receiver.
Courtesy of [30]

The optical receiver consists of two well-matched photodiodes with responsivity close to $1\,A/W$ at 1550nm and an ultra-low noise, high-speed trans-impedance amplifier (TIA) that amplifies the RF heterodyne-detected current obtained from the difference of the photocurrents in the two photodiodes. The use of a trans-impedance amplifier with a high-feedback load resistance ensures a low thermal noise in the receiver. The variable gain op-amp converts the RF current into a voltage signal which is available at the RF

output port of the receiver. Additionally, the unit has two monitor outputs (MONITOR+ and MONITOR-) to observe the optical input power levels on each photodiode separately. These outputs are low-frequency outputs and are used to ensure that the two optical paths are balanced.

The well-balanced photodiodes provide the balanced receiver a common-mode rejection ratio (CMRR) of > 25dB for a carefully balanced-optical link [30]. As shown in the theoretical analysis of balanced coherent detection in section 2.1, the direct-detected currents at the two photodiodes suffer from Relative Intensity Noise (RIN) from the intensity fluctuations at the output of the two lasers. Since the combined field of the two lasers is split using a 3-dB coupler and the total intensity is equally (for an ideal coupler) split and fed into the balanced receiver, noise arising from the intensity fluctuations (RIN) is common between the two branches and is suppressed by the CMRR value. As shown in the system noise analysis in section 6.1, the high CMRR suppresses RIN below LO shot noise and effectively improves the dynamic range of the instrument.

The RF gain of the PDB-150C receiver can be adjusted to 4 different values corresponding to different receiver bandwidths. Table 5.1 shows the different gain values and the corresponding receiver bandwidth. For a 50 Ω load, the gain of the receiver is reduced by half.

Bandwidth (MHz)	Gain (V/A)
0.1	10^7
0.3	10^6
5	10^5
50	10^4

150	10^3

Table 5-1 Different Op-Amp Gain values of the PDB 150C balanced-optical receiver for different receiver bandwidth settings.

The CCA output comprises of the heterodyne-detected signal power within the receiver bandwidth as the LO is swept across the spectrum of the input signal. The bandwidth of the optical receiver thus determines the frequency or wavelength resolution capability, referred to as the resolution bandwidth (RBW) of the instrument. The RBW setting involves a trade-off between frequency resolution and measurement speed. A narrow RBW is desirable for high frequency resolution and better noise performance, while larger RBW results in quicker scan of a wide spectral range. Although the lowest bandwidth setting of the Thorlabs balanced receiver is 0.1MHz, the frequency resolution of the instrument is limited by the LO frequency jitter, which is of the order of 10-15MHz.

The high impedance in the TIA of the balanced receiver ensures a low receiver noise, which is characterized by the Noise Equivalent Power (NEP) value. The minimum reported NEP value for the PDB 150C receiver is $3\,^{pW}/_{\sqrt{Hz}}$ for the frequency range between DC and 10MHz. Figure 14 shows the thermal noise spectrum of the receiver obtained by measuring the spectrum of the output of the receiver with no input optical signal using an RF-SA with a RBW setting of 100kHz. The thermal noise bandwidth corresponds to the gain bandwidth of the receiver. The total receiver noise power for a 50MHz receiver bandwidth setting was measured to be approximately -48dBm, which agrees with the value predicted from the PSD shown in the figure.

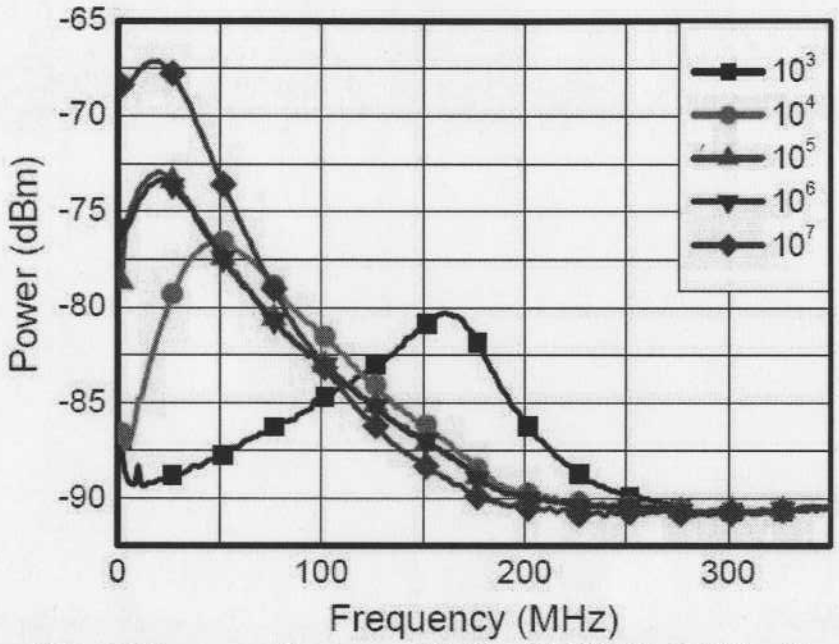

Figure 14. Receiver Noise PSD measured using an RF-SA with 100kHz RBW setting for different gain settings as shown in table 5-1.

Courtesy of [12]

5.3 RF Power Detector and Video Noise

The final stage of a coherent system is the measurement of the heterodyne-detected signal power. In a coherent optical system, such as the CCA, an RF power detector measures the signal and the noise power at the output of the coherent receiver. In this section, we characterize the input-output transfer function of the power-detector used in the experiment. Other properties, such as the dynamic range and output noise of the power detector, are also determined. These properties determine the characteristics such as dynamic range and sensitivity of the CCA.

An AD8362 true rms RF power-detector chip from Analog Devices Inc. was used to measure the heterodyne signal and total bandlimited noise power at the RF output port of the balanced-optical receiver. The power-detector measures the true rms voltage of the RF signal at the input and outputs a DC voltage between 0 and 5V that is proportional to

the logarithm of the signal power. The AD8362 has a 60dB dynamic range, which is the ratio of the largest to smallest measurable signal power, ranging from -52 to 8dBm [31].

With appropriate impedance matching at the input, the AD8362 can measure the power of signals with a bandwidth range from 50Hz to 3.8GHz [31]. The input impedance-matching circuit was configured for low-frequency operation to measure the heterodyne-detected RF signals with a bandwidth corresponding to the optical receiver bandwidth (up to 150MHz). Figure 15 shows the transfer-characteristic of the power detector showing its linear relationship between the input signal power (in dBm) and output voltage. The output power of an RF function generator was swept between -60 and 10dBm for a range of frequencies between 10 and 100MHz and was fed at the input of the power-detector.

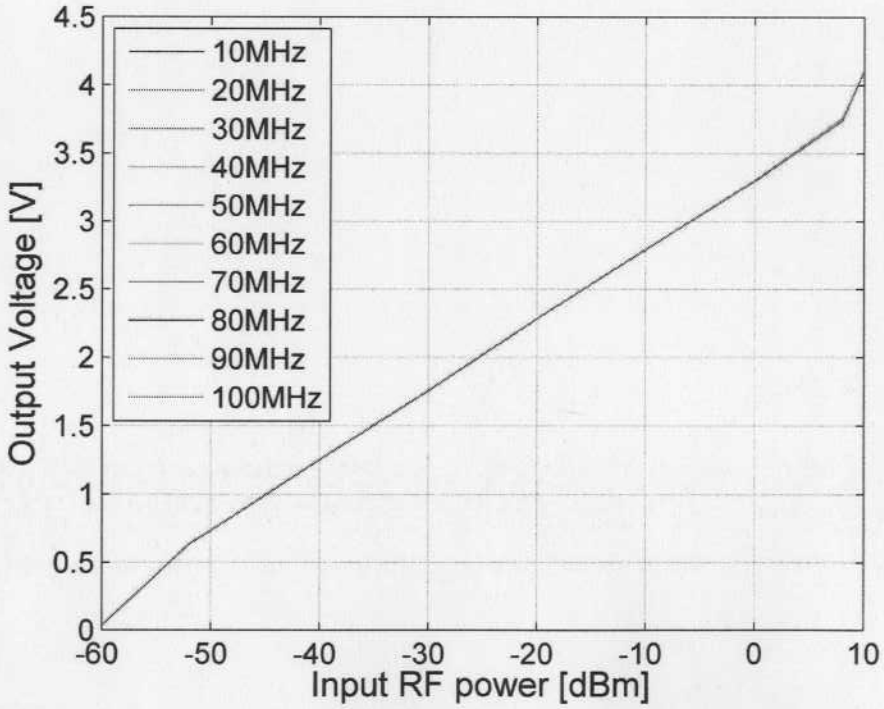

Figure 15. Characterization of the AD8362 RF power detector with input impedance matched for low frequency operation within 100MHz.

From the curves, it can be seen that the input impedance is well matched across the full dynamic range of the power detector for signal frequencies between 10MHz and 100MHz.

The linear relation between the output voltage (v_{out}) of the power detector and the input average RF noise power (P_{in}) can be expressed as

$$v_{out} = k.10\log(P_{in}) + c \quad . \tag{27}$$

From the linear curve fit, the values of k and c were determined experimentally to be $0.0504\,{}^{V}/_{dBm}$ and $2.9V$, respectively.

Fluctuations in the output voltage of the power detector, i.e. output or video noise, limit the sensitivity of the CCA. Eqn. (14) gives the theoretical expression of the output of an

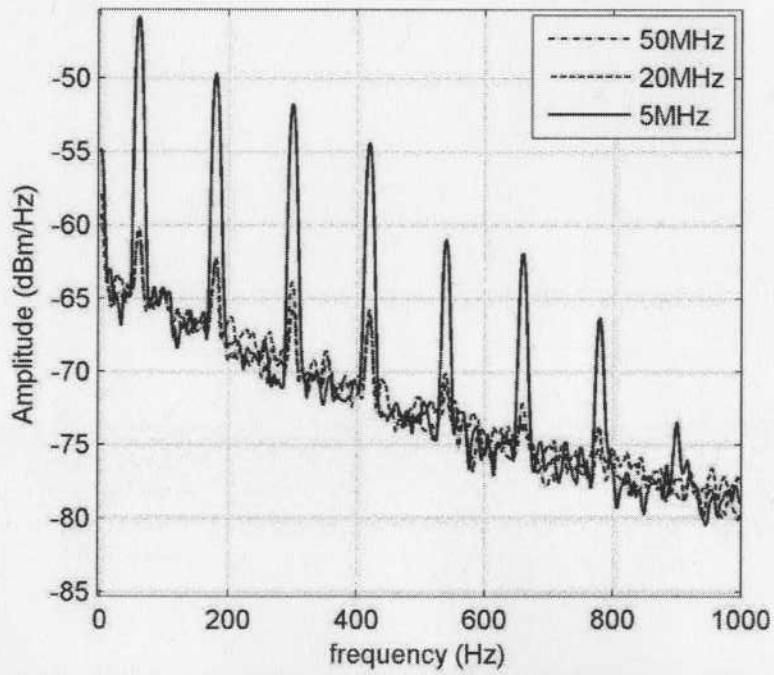

Figure 16. Noise PSD of the output of the AD8362 power detector measuring band-limited noise measured using an RF-SA with 10Hz RBW setting.

ideal square-law power detector with a band-limited white-noise input signal. The AD8362 power detector uses an automatic-gain-control loop that monitors and maintains the measured input RF signal at a constant amplitude level [31]. As a result, the video noise is independent of the average input noise power. Figure 16 shows the measured noise power spectral density at the output of the AD8362 power-detector measuring the thermal noise of the balanced-optical receiver. From the figure, it is clear that the video noise power is independent of the bandwidth of the measured thermal noise. The broad spectral shape is the power detector output-filter response with the spikes seen at odd harmonics of 60Hz power-line frequency. Since the detected noise dominates other noise sources such as flicker noise, modulating the signal to a higher frequency and using a lock-in-amplifier to measure the signal does not improve the sensitivity of the detection.

A Keithley2700 digital multi-meter measures the DC output voltage of the power-detector. The display rate of the instrument is determined by the signal averaging or integration time. The integration time of the multi-meter can be adjusted between 0.03ms to 1s, corresponding to a low-pass filter bandwidth of 30kHz to 1Hz, respectively, which determines the video bandwidth (VBW) of the CCA over which the output signal including video noise (shown in Figure 16) is integrated.

Assuming the video-noise spectrum to be white, the total video noise power can be considered to be proportional to the VBW. The standard deviation σ of the video-noise voltage is then proportional to square-root of the VBW (f_{LP}),

$$\sigma = \sigma_n \sqrt{f_{LP}} \quad . \tag{28}$$

Figure 17 shows the measured standard deviation (σ) of the output of the power-detector measuring the receiver thermal noise power for different values of the VBW.

The solid line denotes the best-curve-fit based on eqn. (28). The departure of the measured standard deviation for VBW values greater than 50Hz is because eqn.(28) assumes a flat power spectral density, whereas from Figure 16, the video noise power decreases with frequency and reduces by 10dB at 400Hz. The value of the video noise voltage density σ_n was thus determined experimentally as approximately $13\ ^{\mu V}/_{\sqrt{Hz}}$ for VBW within 50Hz.

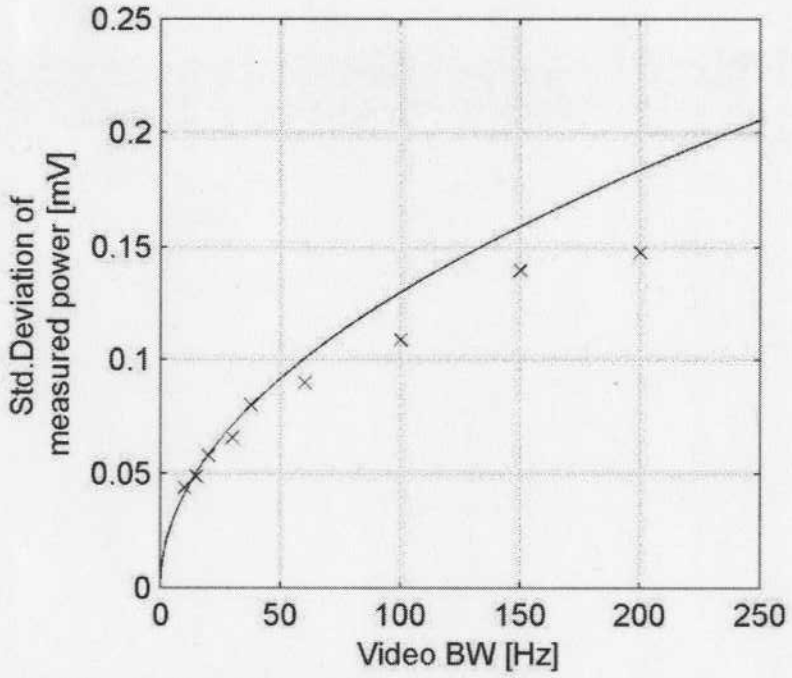

Figure 17. Measured and Theoretical std. deviation of the output of the power detector measuring band-limited noise.

6.0 System Performance Characterization

In previous sections the signal and noise power associated with heterodyne detection of an optical signal was derived. In this section, we derive an end-to-end SNR model for the CCA using the properties of the individual system components that were characterized in section 5. The model provides a complete description of the system and is used to predict the detected output signal and noise power for a given optical signal and LO intensity. Important characteristics related to the performance of the system, such as sensitivity and dynamic range can be obtained from the system model. The output SNR can also be used to determine the required LO intensity for best noise performance.

6.1 Output SNR of the CCA

In the absence of an optical input signal, the RF signal at the output of the balanced receiver is the sum of receiver noise, shot noise and RIN from the LO laser. The DC output voltage (v_1) of the power detector measuring the total RF noise power (P_n) can be expressed as

$$v_1 = k.10\log(P_n) + c \quad . \tag{29}$$

The values of k and c were derived in section 5.3, where the RF power-detector was characterized.

Output noise or video noise of the CCA can be expressed as the standard deviation (σ) of the mean output voltage (v_1) associated with the measurement of the average RF noise power (P_n). As shown in section 5.3, the output video noise spectral density within a 100Hz detection bandwidth (VBW) at DC is approximately $13\,{}^{\mu V}/_{\sqrt{Hz}}$.

With the addition of an RF heterodyne signal (P_s), due to an optical input signal (L_s), the output voltage (v_2) is given by

$$v_2 = k.10\log(P_s + P_n) + c \quad . \tag{30}$$

The RF signal (P_s), shot noise and intensity noise are amplified by the adjustable trans-impedance gain, G of the optical-balanced receiver. A gain setting of $10^4\ {}^{V}\!/_{A}$ on the Thorlabs PDB150C balanced receiver, which corresponds to a 50MHz receiver bandwidth, was used for the experiment. Since the load impedance (Z_L) was $50\,\Omega$, the effective gain was reduced by half. Using Eqn (8), the RF signal power can be expressed as

$$P_s = \frac{(2L_sL_{LO})(G^2)}{Z_L} \quad , \tag{31}$$

where L_s and L_{LO} correspond to the optical signal and LO intensities, respectively.

The CCA output signal is given by the increment (Δv) in the output voltage of the power detector with the addition of the RF heterodyne-signal power (P_s). From the difference in the two output voltages from equations (29) and (30),

$$\Delta v = 10k\log\left(1 + \frac{P_s}{P_n}\right) \quad . \tag{32}$$

For $P_s << P_n$, the expression simplifies to

$$\Delta v = 10k.(0.4343)\left(\frac{P_s}{P_n}\right) \quad . \tag{33}$$

Thus the output signal voltage is directly proportional to the heterodyne-converted RF signal-to-noise power ratio.

The signal-to-noise ratio (SNR) at the output of the detector (hence CCA output) is given by

$$SNR = \frac{\Delta v}{\sigma}, \tag{34}$$

where σ is the video noise, characterized in section 5.3. The low-pass filter bandwidth or video bandwidth (VBW) was set to 100Hz. The VBW can be adjusted by changing the display time on the digital multi-meter. The output SNR can be improved by using a narrow video bandwidth (VBW), but at the expense of the read-out (integration) time of the detector, which determines the speed of the instrument.

Figure 18 shows the theoretical values of the output signal (solid lines) and noise power (dashed lines) vs. LO intensity for a VBW of 100Hz (~0.01s integration or read-out time). The figure shows the linear increase in the output signal with the LO and input

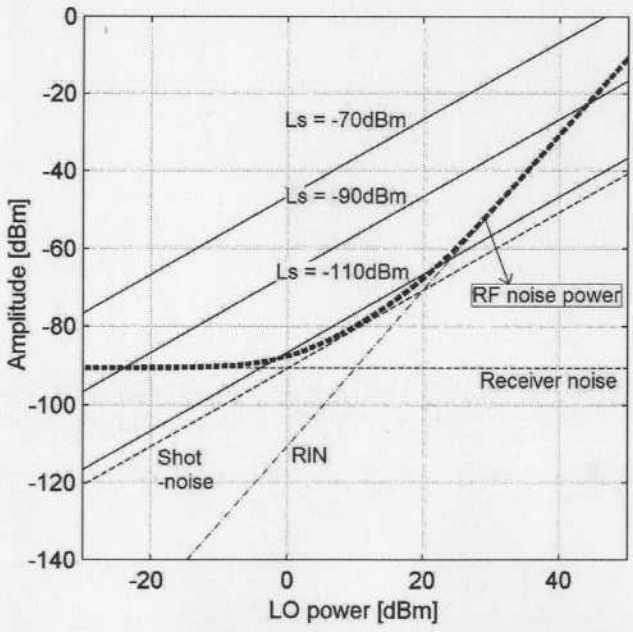

Figure 18. CCA RF signal (solid lines) and Noise power (dashed line) vs. LO power for 50MHz RBW and 100Hz VBW setting.

optical signal intensity (L_s). The dashed line shows the total noise contribution from thermal noise, shot noise and RIN, which are also shown individually. While thermal noise is independent of LO intensity, shot noise varies linearly, and RIN quadratically with LO power. In the LO intensity range between 0 and 15dBm, RIN is suppressed below shot noise due to the -25dB CMRR value of the balanced receiver, assuming perfect balancing of the two channels is achieved.

From the signal and noise-floor characteristic in Figure 18, it can be seen that the SNR improves linearly with LO power until the noise floor is dominated by shot noise, after which the SNR is constant as both noise and signal power increases linearly with the LO. The SNR starts to degrade once the noise power is dominated by RIN, which increases as square of the LO intensity. This is shown more clearly in Figure 19, which plots the SNR vs. LO power for different values of input optical signal intensity. From Figure 19 it is clear that the best SNR performance of the CCA can be achieved for the shot-noise limit when LO power is between 0 and 15dBm.

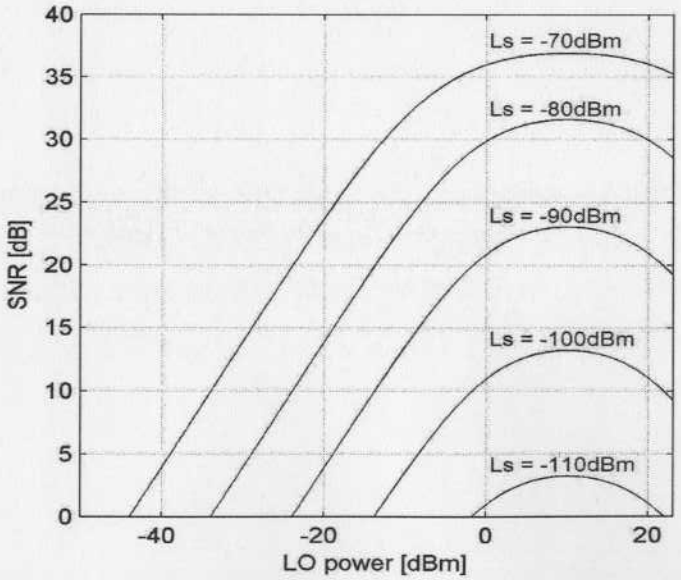

Figure 19. Calculated SNR vs. LO power for different signal powers, with 50MHz RBW and 100Hz VBW setting.

From eqn. (31), it can be seen that the output SNR varies linearly with the input signal intensity. Using the expressions derived above, the output SNR of the CCA can be expressed in terms of the input optical signal power (Ls). Figure 20 shows the theoretical SNR values as a function of the input optical signal intensity for a 50MHz RBW and 100Hz VBW setting, for different values of LO intensities.

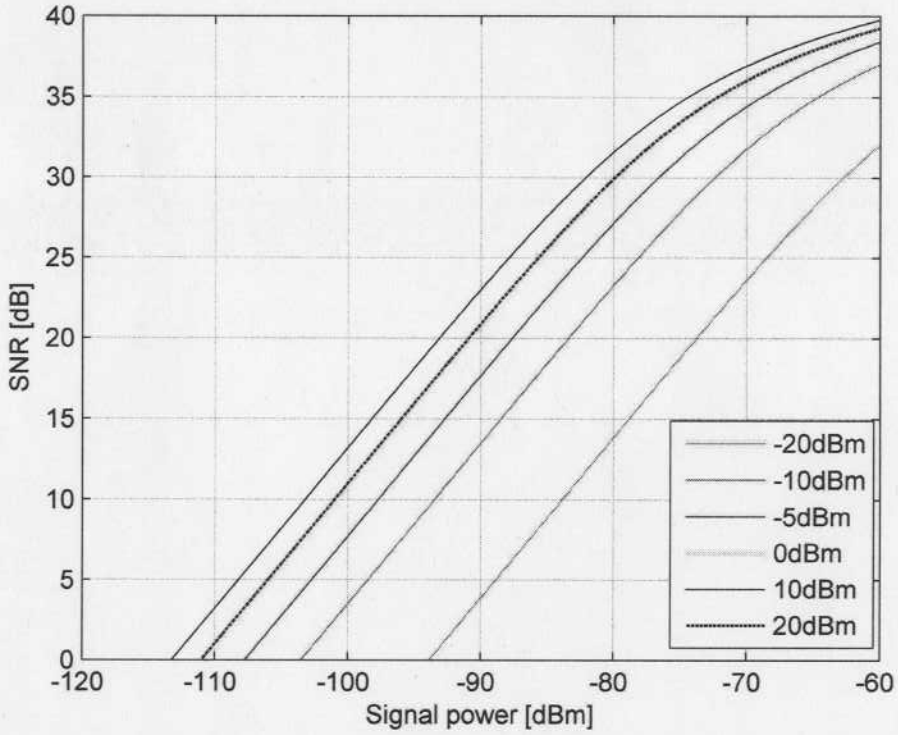

Figure 20. Calculated SNR vs. Input optical signal power for different LO intensities, for 50MHz RBW and 100Hz VBW settings.

One of the advantages of heterodyne detection is its sensitivity. Since the output heterodyne signal is a product of the signal with the LO power, weak signals can often be detected using a strong LO until the noise floor is dominated by shot noise or intensity noise arising from the LO. Thus, generally the measured input optical signal are much weaker than the LO.

As seen in Figure 20, the SNR increases linearly with the input signal intensity. The slope decreases for signal powers resulting in SNR>30dB due to the linear-in-dB transfer characteristic of the RF power-detector. Similar to observations made from Figure 19, the SNR is seen to increase in proportion to the LO power for LO intensities up to approximately 0dBm, when the noise floor is dominated by the thermal noise of the receiver. The SNR increases by 10dB for an increase in LO intensity from -20 to -10dBm. Between 0dBm and 15dBm, when the LO shot noise begins to dominate, the increase in SNR is negligible, and beyond that, the SNR performance decreases when RIN becomes the dominant noise source. As a result, the SNR curves for LO powers of 0 and 20dBm almost overlap each other.

From the graph, the sensitivity limit of the shot-noise-limited CCA is approximately -115dBm for a detection bandwidth of 100Hz. This is explained further in the next section on sensitivity.

Figure 21 shows experimentally measured values of SNR versus input signal power for 2 different values of the LO intensity. Excellent agreement is seen for the two sets of data

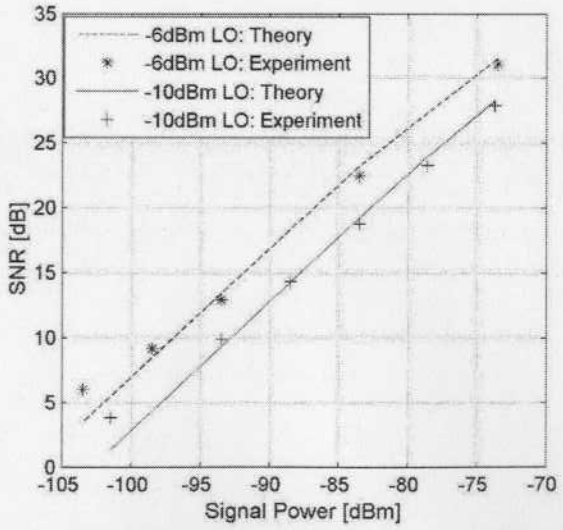

Figure 21. Measured SNR vs. Signal Power for 2 different LO powers.

with the predicted values from the theoretical model. For the weak LO intensities used in the experiment, the dominant noise term was thermal noise, as characterized in Figure 18. Better sensitivity can be achieved if more LO power was available.

6.2 Sensitivity of the CCA measurement

In this section, we determine the minimum detectable input optical signal power. The sensitivity of the CCA is defined as the optical signal power resulting in an output SNR of 1 or in other words, the mean output voltage (Δv) is equal to 1x the output rms noise voltage (σ). Equating the expression for output SNR given by eqn. (34) to one, we get

$$P_s = \left(10^{\frac{\sigma_n \sqrt{f_{LP}}}{10.k}} - 1 \right) P_n \quad . \tag{35}$$

Eqn. (35) relates the sensitivity of the RF power detector to the average noise power (P_n) being measured, the video-noise power spectral density (σ_n) and the detection bandwidth or VBW (f_{LP}) at the output of the RF power detector.

The sensitivity of the CCA can be obtained using the relation between the input optical signal and the heterodyne-detected RF signal power as described by eqn. (31). The resulting expression for the sensitivity of the CCA is given by

$$L_{s\_\min} = \frac{Z_L}{2L_{LO}G^2} P_n \left(10^{\frac{\sigma_n \sqrt{f_{LP}}}{10.k}} - 1 \right) \quad . \tag{36}$$

Thus the sensitivity of the CCA can be expressed in terms of the LO intensity, the balanced receiver gain setting (G), load resistance (Z_L), RF noise power (P_n) and the video-noise ($\sigma_n \sqrt{f_{LP}}$). For a gain setting of $10^4\ {}^{V}/_{A}$ (50MHz receiver bandwidth) and a load resistance of 50Ω, the sensitivity of the CCA can be expressed in dBm as

$$L_{s\_\min}(dBm) = P_n(dBm) + 10\log\left(10^{\frac{\sigma_n\sqrt{f_{LP}}}{10.k}} - 1\right) - 30dB - L_{LO}(dBm) \quad (37)$$

Figure 22 shows the noise floor measurement of the CCA for three different values of VBW and demonstrates the relationship expressed in eqn. (37). The experimental setup

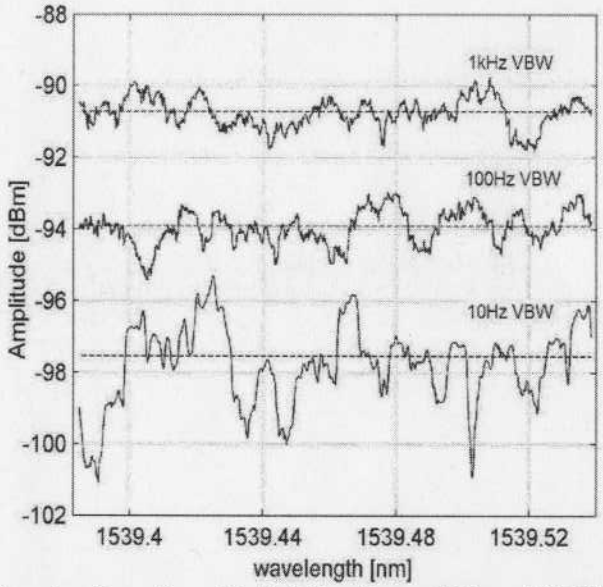

Figure 22. CCA noise floor (sensitivity) for three different VBW values averaging over 50samples and LO intensity of -20dBm.

of figure 10 was used without an optical input signal and the LO power was limited such that the receiver thermal noise was the dominant noise factor. The straight dashed lines denote the predicted noise floor of the CCA based on eqn. (37), for a measured thermal noise of -50dBm and a local oscillator power of -20dBm.

6.3 Dynamic Range

The dynamic range of the CCA is the ratio of the largest to the smallest measurable signal power. As shown in previous sections, the relationship between the optical and RF signal powers is linear, while the input-output relationship of the RF-power detector is

logarithmic. Eqn. (33) relates the output signal voltage (Δv) to the RF signal (P_s) and noise (P_n) power.

The lower limit of the dynamic range corresponds to the signal power for an output SNR of 1. Similar to the analysis of sensitivity shown in section 6.2, we equate the output signal voltage to the video or output noise (σ), which was characterized in section 5.3.

The upper limit of the dynamic range can be obtained, again, by using eqn. (33) and assuming the RF signal power is much larger than the noise power at the output of the balanced receiver, i.e., $P_s >> P_n$, such that

$$\Delta v_{\max} = 10k \log\left(\frac{P_{s\_\max}}{P_n}\right) \quad . \tag{38}$$

The dynamic range of the CCA can be derived from the ratio of the signal powers corresponding to the maximum and minimum output signal voltages:

$$DR = \frac{P_{s\_\max}}{P_{s\_\min}} = \frac{10^{\Delta v_{\max}/10k}}{10^{\sigma\sqrt{f_{LP}}/10k} - 1} \tag{39}$$

From eqns. (38) and (39), the dynamic range of the CCA depends on the dynamic range and video noise of the RF power detector. Assuming the entire dynamic range of the AD8362 power detector is used and the video bandwidth is 100Hz, the dynamic range of the CCA is evaluated from eqn. (39) to be 92dB.

7.0 Spectral Measurements

7.1 CW-ECT laser spectral measurement

The experimental setup shown in

Figure 10 was used without the electro-optic phase modulator to measure the CW spectrum of a tunable Agilent ECT laser with a center frequency of approximately 1539nm. Figure 23 shows the heterodyne-detected RF signal power measurement for

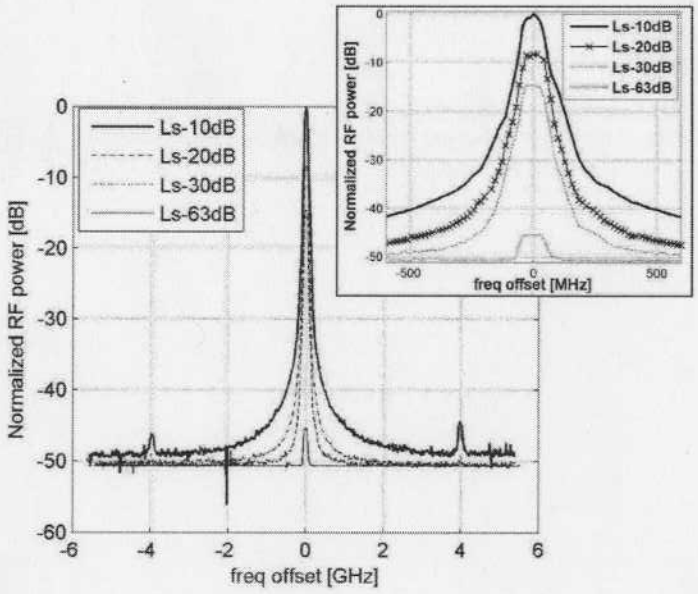

Figure 23. Detected power of RF-heterodyne signal corresponding to a CW-ECT laser using a DFB LO (denoted Ls in the figure) with different attenuation settings.

different values of attenuation of the optical signal intensity (L_s).

As expected, the RF signal power varies linearly with the input optical signal power. The inset figure shows how the peak of the heterodyne-detected RF signal reduces by 10dB corresponding to a 10dB decrease in the optical signal.

The heterodyne conversion of the phase noise of the DFB laser used as the LO is evident from the broad Lorentzian shape in the measured spectrum. Characterization of

the CCA output for the intensity-converted phase noise from the LO and the corresponding loss in sensitivity is discussed in section 3.2. For strong LO signals, weak side-modes of the tuneable ECT laser can be observed at 4GHz. The weakest optical signal intensity that can be measured is characterized by the sensitivity of the CCA, which was described in section 6.2.

7.2 Phase-modulated ECT laser spectral measurement

The increase in demand on bandwidth has led to investigation of advanced modulation techniques such as multi-level phase modulation where signal information is transmitted by modulating the phase of the carrier with the desired signal. Such techniques are more spectrally efficient than the traditional on-off keying method which does not utilize the phase of the carrier. The intensity spectrum of a phase-modulated signal consists of side-bands around the carrier, symmetric in amplitude and separated by the modulating frequency.

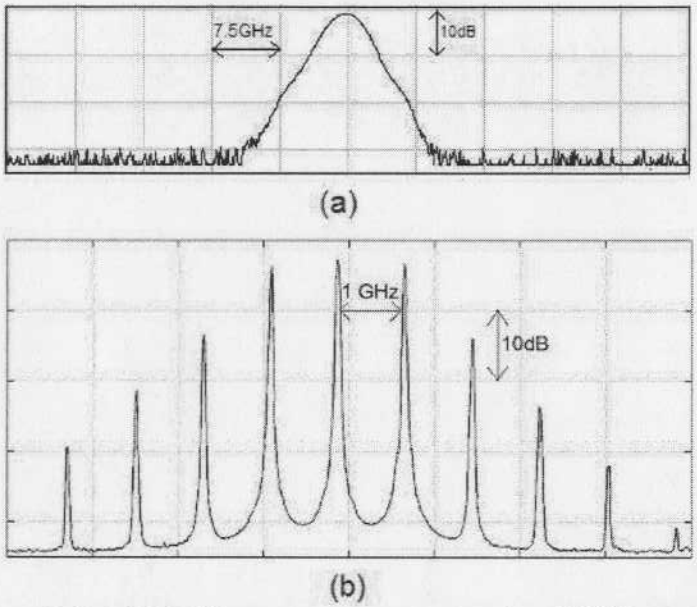

Figure 24. Phase modulated ECT laser spectrum centered at 1539.5nm observed using an Agilent grating-based OSA (a) and the proposed CCA (b).

Figure 24 shows the spectrum of a 1GHz phase-modulated ECT laser measured using the CCA. The spectrum shows the center frequency of the ECT laser and the sidebands separated by the modulating frequency. The figure also shows the improvement in resolution over a grating-based Agilent optical spectrum analyzer E86140B measuring the same optical spectrum using its narrowest resolution of 0.06nm (7.5GHz at 1550nm). Clearly, coherent detection offers substantial advantages in resolution of essential spectral features. Also, the impact of phase noise of the DFB LO causing the spectral broadening is evident between the sidebands. While the use of an ECT laser as the LO would have improved the measured spectrum, a wide field of use could exist for the CCA, given the low cost and small size of the TT-DFB.

Resolution bandwidth (RBW) of a spectrum analyzer is a measure of the minimum frequency separation for the instrument to differentiate between two spectral features. RBW of the CCA is determined by the optical receiver BW. The minimum RBW of the

CCA is limited by the LO frequency jitter, which is of the order of 10 to 15MHz. Figure 25 (a) to (d) shows the measurement of an ECT laser phase-modulated with different modulation frequencies, using the CCA with the bandwidth of the optical receiver set to 50MHz (RBW) and a LO-intensity of -15dBm. The figure demonstrates that with the resolution bandwidth of the CCA set to 50MHz, modulation sidebands that are 100MHz (twice the optical receiver bandwidth) apart or more can be clearly resolved. In addition, side-modes of the ECT laser can be seen at about 4GHz from the central peak.

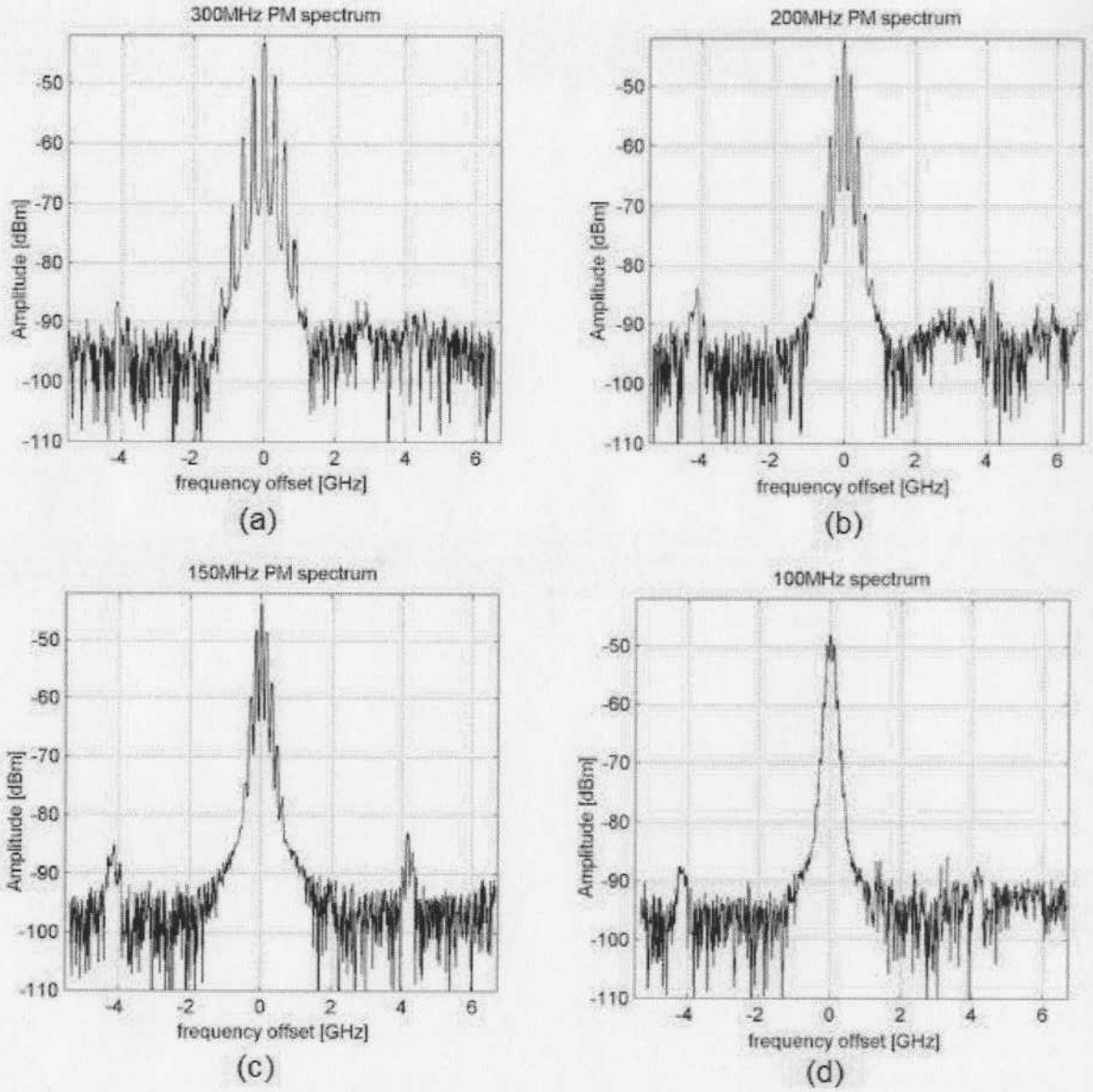

Figure 25. CCA measurement of a phase-modulated ECT laser at 1536nm demonstrating a frequency resolution capability of 100MHz.

The loss in detectability of weak sidebands in the vicinity of a strong carrier due to phase noise of the DFB laser is demonstrated in Figure 26. Two 200MHz phase-modulated ECT laser spectra with sidebands of different powers relative to the carrier are compared. The figure shows that the detection of a weak sideband 200MHz away from

the carrier and with power 20dB lower than the carrier (dBc) is limited by the converted LO phase noise associated with a strong neighbouring carrier.

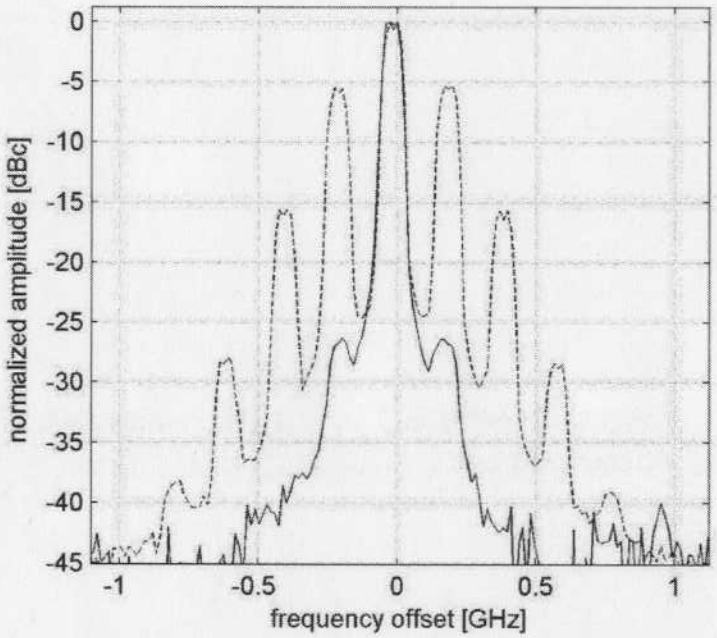

Figure 26. Comparison of CCA spectral measurement of two 200MHz phase-modulated ECT lasers with different modulation indices.

This limitation is consistent with the converted phase-noise floor of the CCA output as characterized in section 3.2. The graph in Fig. 27 is obtained from eqn. (26) and shows the noise floor at the output of the CCA due to the converted phase noise of the LO in detecting a strong signal in the case where the thermal noise is the dominant electrical noise source at the receiver. The graph is used to characterize the minimum frequency separation required to detect a weak narrow spectral feature such as a weak sideband in a phase-modulated spectrum in the presence of strong carrier 50dB above the thermal noise floor of the receiver. The effect is similar to that of cross-talk between closely spaced channels where power from a strong signal leaks into an adjacent channel, affecting the

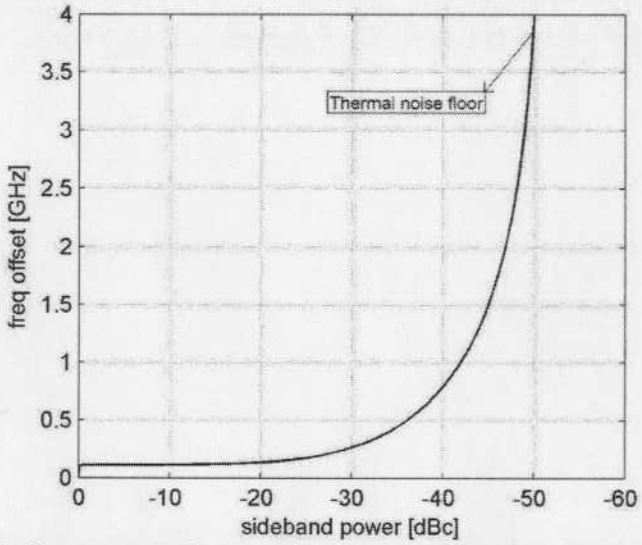

Figure 27. Min freq. separation required to detect a sideband in the presence of a strong carrier 50dB above the thermal noise floor of the receiver.

detection of weak signals. This graph shows that the degradation in signal-to-noise ratio caused by the phase noise of the DFB laser is a concern only in the detection of weak signals (less than -20dBc) in close proximity (within 2GHz) to a strong signal.

8.0 Conclusions

We have built and tested a coherent channel analyzer with high optical frequency resolution that uses low-cost and easily integrable system components. The CCA has been shown to provide comparable frequency resolution to similar high-performance optical spectrum analyzers (HRSA) at a fraction of the cost and size. Experimental measurements of various optical signal spectra demonstrated a frequency resolution capability of 100MHz, sensitivity of -95dBm and a 90dB dynamic range over the tuning range of the LO, which can cover up to ten 50GHz-spaced DWDM channels. The resolution bandwidth can be further improved to 20MHz, limited by the frequency jitter of the LO. The sensitivity of the system can be improved by up to 20dB corresponding to the shot-noise limit using a LO with higher power and improved balancing at the balanced-optical receiver.

9.0 Contributions

The major contributions of this thesis towards the field of high-resolution optical channel analysis are

- The realization of the concept of a **size and cost-effective solution** for various applications that need the high resolution, but not necessarily the broad tuning range and high-performance of a HRSA.
- **Quantitative understanding** of the primary limitations of the use of a DFB laser as a local-oscillator.
- **Theoretical analysis** of the impact of LO intensity and phase noise in optical heterodyne detection was done and its impact on the CCA-measured spectrum was studied.
- Individual components of the CCA were characterized and a complete **end-to-end system model** was provided. The output SNR, sensitivity and dynamic range was obtained using the derived system model to characterize the performance of the CCA.

10.0 Future Work

The dependence of DFB laser frequency on the temperature and drive current of the laser is a well-studied property. However, due to the lack of a suitable control system to perform a controlled frequency sweep of the DFB laser, we have performed the experiments by sweeping the signal spectrum (in this case, a tuneable Agilent ECT laser) across the frequency of the DFB laser. Future work will require the implementation of a control loop providing a feedback mechanism to adjust the temperature and drive-current of the DFB laser to perform a controlled frequency sweep.

Balancing of the optical receiver can be further improved using software for more effective RIN suppression for scenarios when RIN from a high intensity input-signal can dominate the noise floor.

The performance of the CCA can be further quantified by studying the impact of factors affecting the amplitude accuracy, such as, sweep speed, LO phase noise and receiver bandwidth.

Future revisions of the CCA may also include a polarization-diverse architecture to minimize the dependence of the spectral amplitude measurement on the polarization state of the measured signal.

List of References

[1] P.J. Winzer and R.J. Essiambre, "Advanced Optical Modulation Formats", Proceedings of the IEEE, vol. 94, 2006

[2] Agilent 86142 and 86146B Optical Spectrum Analyzers Technical Overview, http://cp.literature.agilent.com/litweb/pdf/5980-0177E.pdf .

[3] S. Yoshida, Y. Tada, and K. Nosu, "High resolution optical spectrum analysis by coherent detection with multi-electrode DBR-LD's as local oscillators," in *Conf. Proc. IMTC/94. IEEE Instrumentation Measurement Technology Conf., vol. 1, 1994, pp. 230–233.*

[4] T. Kataoka and K. Hagimoto, "High resolution optical spectrum analyzer using a heterodyne detection technique," in *Conf. Proc. IMTC/94. IEEE Instrumentation Measurement Technology*, vol. 1, 1994, pp. 234-237.

[5] D. M. Baney, B. Szafraniec, and A. Motamedi, "Coherent optical spectrum analyzer," *Photonics Technology Letters*,vol. 14, pp. 355–357, 2002.

[6] B. Szafraniec et.al, "Swept Coherent Optical Spectrum Analysis," IEEE Transactions on Instrumentation and Measurement, vol. 53, 2004, pp. 203-215.

[7] G.P. Agrawal, *Lightwave Technology,* (John Wiley & Sons, Inc., Hoboken, NJ, 2005), Chap. 1, 3, 4.

[8] G.P. Agrawal, *Nonlinear Fiber Optics,* (Elsevier, Inc., 2007), Chap. 3.2

[9] A.R. Chraplyvy, "Limitations on Lightwave Communications Imposed by Optical-Fiber Nonlinearities", Journal of Lightwave Technology, vol.8, 1990, pp.1548-1558]

[10] J.M. Subías Domingo, J. Pelayo, F. Villuendas, C.D. Heras, and E. Pellejer, "Very High Resolution Optical Spectrometry by Stimulated Brillouin Scattering," *Photonics Technology Letters,* vol. 17, pp. 855-857, 2005.

[11] R.Y. Chiao, C.H. Townes and B.P. Stoicheff, "Stimulated Brillouin scattering and coherent generation of intense hypersonic waves", Physical Review Letters, vol. 12, 1964, pp. 592-595.

[12] A. Yeniay, M.-M. Delavaus, and J. Toulouse, "Spontaneous and stimulated Brillouin scattering gain spectra in optical fibers", Journal of Lightwave Technology, vol. 20, 2002, pp. 1425-1432.

[13] "External-cavity Diode Lasers", Encyclopedia of Laser Physics and Technology, http://www.rp-photonics.com/external_cavity_diode_lasers.html

[14] "Distributed Feedback Lasers", Encyclopedia of Laser Physics and Technology, http://www.rp-photonics.com/distributed_feedback_lasers.html

[15] C. Henry, "Phase noise in semiconductor lasers", Journal of Lightwave Technology, vol.4, 1986, pp.298-311]

[16] J. Posthumus, A. Deninger, and F. Lison. "Distributed Feedback Diode Lasers: Spectral properties and current applications". Toptica Photonics AG.

[17] H. R. Carleton and W. T. Maloney, "A balanced optical heterodyne detector", Applied Optics, vol. 7, 1968, pp. 1241.

[18] R. Stierlin *et al.*, "Excess-noise suppression in a fibre-optic balanced heterodyne detection system", Opt. Quantum Electron, vol.18, 1986, pp. 445.

[19] G.P.Agrawal, *Fiber-Optic Communication Systems* (John Wiley & Sons, Inc., New York, 2002), Chap. 4, 10.

[20] J.B. Johnson, Physical Review Letters, vol. 57, 1928, pp. 541.

[21] H. Nyquist, Physical Review Letters, vol. 32, 1928, pp. 110.

[22] F.N.H. Robinson, *Noise and Fluctuations in Electronic Devices and Circuits,* (Oxford University Press, Oxford, 1974).

[23] G.P. Agrawal and N.K. Dutta, *Long-Wavelength Semiconductor Lasers* (New York: Van Nostrand Reinhold Electrical/Computer Science and Engineering Series, 1986, ch. 6.

[24] S. Stanimirovic et.al, "Measurement in Radio Astronomy". Astronomical Society of the Pacific Conference Series, vol.278, 2002, pp. 81-90.

[25] T. Okoshi, K. Kikuchi, A. Nakayama, "Novel Method for High Resolution Measurement of Laser Output Spectrum," *Electronics Letters,* vol. 16 (1980) 630.

[26] J.A. Armstrong, "Theory of interferometric analysis of laser phase noise", Journal of Optical Society of America, vol. 56, 1966, pp. 1024-1031.

[27] P. Gallion and F. J. Mendieta and R. Leconte, "Single-frequency laser phase-noise limitation in single-mode optical fiber coherent detection systems," Proc. European Conf. Opt. Syst. Appl., Edinburgh, Scotland, 1982, also, Proc. SPIE, Washington, DC, 1983.

[28] H. E. Rowe, *Signal and Noise in Communication Systems.*(Princeton, NJ: Van Nostrand, 1965).

[29] J. Zhang, "Intensity Noise Induced by Stimulated Brillouin Scattering in Optical Fiber Transmission Systems," Ph.D. dissertation, Dept. Elect. And Computer Eng., Northwestern Univ., Evanston, IL, 2005

[30] Thorlabs Balanced Amplified Photodetector schematic, http://www.thorlabs.com/NewGroupPage9_PF.cfm?Guide=10&Category_ID=218&ObjectGroup_ID=1299

[31] Analog Devices, Inc. AD8362 true-rms power detector data sheet, http://www.analog.com/static/imported-files/data_sheets/AD8362.pdf